crystals

MDPI

Review

Properties and Applications of Flexible Poly(Vinylidene Fluoride)-Based Piezoelectric Materials

Linfang Xie [1], Guoliang Wang [1], Chao Jiang [2], Fapeng Yu [1,*] and Xian Zhao [1,2,*]

[1] State Key Laboratory of Crystal Materials and Institute of Crystal Materials, Shandong University, Jinan 250100, China; 202012900@mail.sdu.edu.cn (L.X.); wangguoliangzyj@126.com (G.W.)
[2] Key Laboratory of Laser & Infrared System, Ministry of Education, Shandong University, Qingdao 266237, China; yjr625682805@163.com
* Correspondence: fapengyu@sdu.edu.cn (F.Y.); xianzhao@sdu.edu.cn (X.Z.)

Abstract: Poly (vinylidene fluoride) (PVDF) is a kind of semicrystalline organic polymer piezoelectric material. Adopting processes such as melting crystallization and solution casting, and undergoing post-treatment processes such as annealing, stretching, and polarization, PVDF films with high crystallinity and high piezoelectric response level can be realized. As a polymer material, PVDF shows excellent mechanical properties, chemical stability and biocompatibility, and is light in weight, easily prepared, which can be designed into miniaturized, chip-shaped and integrated devices. It has a wide range of applications in self-powered equipment such as sensors, nanogenerators and currently is a research hotspot for use as flexible wearable or implantable materials. This article mainly introduces the crystal structures, piezoelectric properties and their applications in flexible piezoelectric devices of PVDF materials.

Keywords: poly(vinylidene fluoride); self-powered equipment; crystal structures; piezoelectric properties; piezoelectric devices

Citation: Xie, L.; Wang, G.; Jiang, C.; Yu, F.; Zhao, X. Properties and Applications of Flexible Poly(Vinylidene Fluoride)-Based Piezoelectric Materials. *Crystals* **2021**, *11*, 644. https://doi.org/10.3390/cryst11060644

Academic Editor: Pankaj Sharma

Received: 13 May 2021
Accepted: 2 June 2021
Published: 6 June 2021

1. Introduction

In 1880, French scientists Pierre Curie and Jacques Curie discovered the piezoelectric effect that applying force to crystals with non-centrosymmetric structures along a specific direction will generate electric charges on the surface of zinc blende, sodium chlorate, boracite, tourmaline, and crystal quartz [1]. The discovery opened the prelude to the research of piezoelectric materials. According to the structural symmetry, the crystal materials can be divided into 32 point groups. Among them, 21 kinds have non-centrosymmetric structures and exhibit piezoelectricity, except for the 432 point group with high symmetry. Piezoelectric materials are mainly divided into inorganic piezoelectric materials, such as piezoelectric single crystals, ceramics, metal oxides, organic polymer piezoelectric materials, such as nylon-11 [2], polylactic acid [3], polypropylene [4], poly(vinylidene fluoride) (PVDF) [5] and its copolymers, and organic–inorganic composite piezoelectric materials. Inorganic piezoelectric materials are a type of piezoelectric materials that have been discovered and applied earlier, but due to their brittleness, hardness and the complex processing, their applicability in the field of flexible, miniaturized, and integrated devices is limited [6]. Among the organic polymer piezoelectric materials, PVDF and its copolymers exhibit the best piezoelectric properties among the current piezoelectric polymers [7–11], considered to be one of the most feasible alternatives to piezoelectric ceramics.

PVDF is a kind of semicrystalline polymer. In 1969, Japanese scientist Kawai found that PVDF has stronger piezoelectricity after being mechanically stretched and high-voltage polarization [12]. Compared with other polymers such as poly(vinyl chloride) and polycarbonate, it has more outstanding piezoelectric activity, this discovery means that piezoelectric historical progress has taken place in polymer research. After that, the researchers also found that PVDF and its copolymers also have good pyroelectric and ferroelectric

behaviors [13–16]. Its excellent electrical properties have greatly broadened the application fields of PVDF materials.

Currently, the electronic devices are developing towards the tendency of miniaturization, light weight, and intelligence, which exhibits higher requirements to the performance and processability of piezoelectric materials. PVDF and its copolymers have the advantages of excellent flexibility, light weight, high piezoelectric response, good chemical stability, biocompatibility and nontoxicity [17]. It is deemed as an promising candidate for self-powered intelligent electronic devices which convert weak mechanical energy into electrical signals that have great potential in sensor applications [18–22], energy harvesting and storage devices [23–29], and biomedical materials [30–33], especially in the field of wearable or implantable devices. At present, many studies are mainly focusing on improving the performance by changing the material structure, the design and optimization of the device microstructure, and the exploration of high-performance, multifunctional devices [29,34–37]. The combination of the application of flexible piezoelectric materials and information technology can promote the information interaction between people and things, improve the efficiency of information acquisition, and promote the development of the Internet of Things. More and more, the PVDF and its copolymers become a very important piezoelectric system.

In this paper, we discuss the structures of each phase of PVDF and the three commonly used methods to characterize the crystal structure, X-ray diffraction (XRD), Fourier transform infrared spectroscopy (FTIR) and differential scanning calorimetry (DSC). In addition, the piezoelectricity of PVDF and its copolymers are introduced and some methods which can improve the performance of PVDF to facilitate readers to better understand the piezoelectric properties of PVDF and its copolymers are summarized. Moreover, several typical applications of PVDF-based piezoelectric materials in sensors, nanogenerators, and biomedical materials are presented.

2. Crystal Structures and Characterization of PVDF

2.1. Crystal Structures

PVDF is a linear semicrystalline polymer with crystalline phase coexisting with amorphous phase. The molecular weight is in the order of 10^5 and the crystallinity is about 50%. The internal rotation of the single bond of the polymer will cause the difference between the structures of the molecular backbone and the spatial arrangements of the groups. Therefore, the PVDF molecular chain will exhibit different conformations and have multiple phase structures. There are five PVDF phase structures discovered so far, α phase (crystal form II), β phase (crystal form I), γ phase (crystal form III), δ phase (crystal form IV) and ε phase (crystal form V) [38]. Table 1 shows the unit cell parameters.

Table 1. The unit cell parameters of the common crystal phases of PVDF [39–41].

Phase	Conformation	Space Group	Symmetry	Cell Parameters (Å)
α	TGTG′	$P2_1/c$	Monoclinic	a = 4.96, b = 9.64, c = 4.62 β = 90°
β	TTT	$Cm2m$	Orthorhombic	a = 8.58, b = 4.91, c = 2.56
γ	T_3GT_3G'	Cc	Monoclinic	a = 4.96, b = 9.58, c = 4.23 β = 92.9°
δ	TGTG′	$P2_1cm$	Monoclinic	a = 4.96, b = 9.64, c = 4.62 β = 90°

The molecular chain structure and lattice constant of the α phase and the δ phase are similar, and they are both in the helical conformation (TGTG′) [40,42]. The TGTG′ conformation is polar, but because of the inclination of dipoles to the molecular axis, it has components of the net moment both perpendicular and parallel to the chain that leads to a smaller polarity of the chain [5]. However, there is a difference in the arrangement of the molecular chains between the α phase and the δ phase. The two molecular chains in the

unit cell in the α phase are stacked in an antiparallel manner, the dipole moments mostly cancel out each other, thus no net dipole moment remains [5]; while for the δ phase, the two molecular chains in the unit cell are arranged in an up–down pattern, the dipole moments of the molecular chains are parallel and show a distinct net dipole moment. Under the condition of applying an electric field, the transformation from α phase to δ phase can also be realized [40]. In the β phase, the molecular chain is in a plane zigzag all-trans conformation (TTT) [39,43], the -CF_2- group and -CH_2- group on the molecular chain are facing one side each, and the dipole moments are arranged in parallel and perpendicular to c axis, this conformation is the most highly polar conformation. Considering the steric hindrance of the fluorine atoms in the molecular chain, Hasegawa et al. [39] proposed an alternately deflected molecular chain structure, which can reduce the steric hindrance between fluorine atoms and lower the molecular potential energy. The γ phase crystal structure can be regarded as the deformation of the β phase crystal structure, which can be obtained by high-pressure heat treatment and casted in the organic solvent dimethyl sulfoxide or dimethylacetamide [41]. The polarity of the γ phase is second only to the β phase. Lovinger [44] found that the polar homologue of the α phase, the δ phase, is prone to phase transition at high temperature when studying the annealing behavior of PVDF films, resulting in a polar phase γ phase and a small amount of non-polar ε phase [45]. The mixture verifies the existence of the ε phase. The conformation of the ε phase and the γ phase is the same as T_3GT_3G', but the molecular chain stacking method is similar to that of the α phase, which is a non-polar phase. Due to the small difference in potential energy between the various conformations of PVDF, it is easy to undergo phase transition under external conditions such as heat treatment, pressure, and electric field. Figure 1 gives two common molecular structures of PVDF.

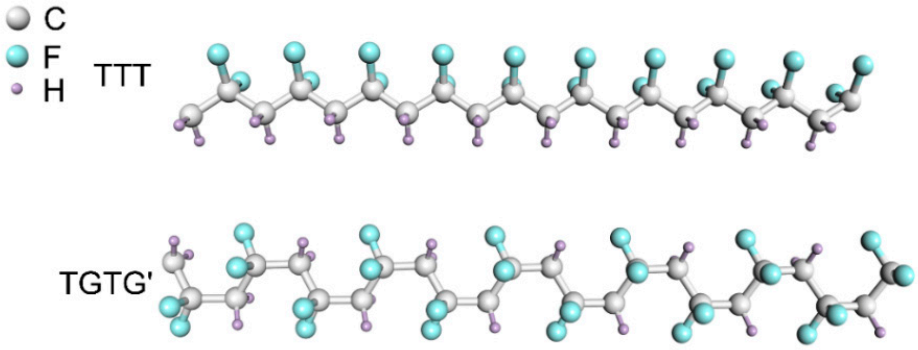

Figure 1. All-trans conformation (TTT) in α phase and helical conformation (TGTG') in β phase.

The TrFE (trifluoroethylene) and CTFE (chlorotrifluoroethylene) units are introduced into PVDF to obtain binary or terpolymers. Compared with the H atom, the F atom has a larger size, so the introduction of these units will produce greater steric hindrance, which will help the formation and stability of the all-trans chain structure (β phase) [5,46]. These copolymers mainly have three phase structures, the low-temperature (LT, a crystalline phase similar to the polar orthorhombic β phase) phase [47,48], the high-temperature (HT, the packing of conformationally disordered chains in hexagonal structure) phase, and the cooled phase (CL, a kind of superlattice consists of the domains of long trans chains linked together with the boundaries of disordered trans-gauche bonds), the phase transition occurs among them during thermal treatment process [49–51]. Phase transition is closely related to content of TrFE or CTFE units [17,52,53]. In P(VDF-TrFE) copolymers with 50~60 mol% VDF molar, the LT phase transforms into the CL phase during the heating process, and the CL phase continuously transforms into the HT phase. Transitions between the phases are definite; however, for the copolymer with lower amounts of VDF less than 40 mol%, there is a broad transition between the CL and HT phases, when the content of VDF up to 70~80 mol%, a clear and discontinuous first order transition between the LT and HT phases is observed and the CL phase does not practically appear [47]. It is worth mentioning

that when the P(VDF-TrFE) undergoes annealing treatment above the Curie temperature and cooling back, a defective ferroelectric (DFE) phase would appear in addition to the ferroelectric (FE) phase [51]. Subsequently, the DFE phase can be transformed into the FE phase when polarized at room temperature, leading to a significant increase of the ferroelectric phase content [51]. P(VDF-TrFE-CTFE) copolymers with CTFE content from 0 to 10 mol% mainly exhibit ferroelectric or relaxor ferroelectric (RFE) properties at low temperatures whereas they all present paraelectric (PE) behavior at high temperatures [54]. What is more, the phase transitions are also affected by various amounts of CTFE units in the thermal evolution of this relaxor ferroelectric terpolymers. For the terpolymer with 9.7 mol % of CTFE, there is a continuous phase transition (RFE to PE), however, for the composition (4.4 mol % CTFE), a discontinuous transition occurs (FE to PE) and the RFE to PE and FE to PE phase transitions coexist [55]. Meanwhile, the thermo-mechanical and dielectric properties evolve continuously with CTFE content and their evolutions are linked to the structural properties [54].

2.2. Characterization Methods

The characteristic of crystallization of PVDF is the coexistence of crystalline and amorphous regions. The XRD [43,56–59], FTIR [60–66] and DSC [24] are the methods commonly used for qualitative or quantitative analysis of different phase structures. In early research, XRD was used to analyze the structure of each phase of PVDF, to obtain information such as conformation, unit cell parameters, space group, etc. In subsequent studies, the phases and crystallinity are often judged based on the characteristic peaks in the diffraction pattern. PVDF containing a single β phase can be obtained by solvent crystallization, the diffraction pattern produces a sharp absorption peak at $2\theta \approx 20^\circ$, which represents the sum of the diffraction intensity of (1 1 0) and (2 0 0) planes. Similarly, the characteristic diffraction peaks of α phase can be obtained, the absorption peaks at approximately $2\theta = 17.66^\circ$, 18.30°, 19.90° and 26.56° [56]. Lopes et al. obtained a single γ phase by adding rare earth elements and obtained diffraction patterns, when the samples are melted at 200 °C, the XRD patterns show the peaks at 18.5°, 19.2°, 20.1°, 20.3°, and 26.8°, characteristic of the γ phase [57].

There are three types of absorption peaks in the infrared spectra, such as the common absorption peaks of the three phases, the characteristic absorption peak of only one phase, or the double peaks produced by the two phases [66]. The characteristic absorption peaks can be used to distinguish each crystal phase, and then calculate the content of each phase in the mixture. However, the positions of some characteristic peaks are very close, especially the β phase and the γ phase which have very similar conformations, so there are many statements on the selection of characteristic peaks. For example, in some research, the positions of 510 and 840 cm^{-1} peaks can be used to characterize individual β phase or γ phase [61,62], or the common peak of the two [60,65]. Cai et al. [66] compared the characteristic absorption peaks of each phase and proposed to judge the existence of α phase by the peaks at 763 and 614 cm^{-1}, and the peak at 1275 cm^{-1} to judge the existence of β phase, the 1234 cm^{-1} to the γ phase. The characteristic peaks of β phase and γ phase are combined to determine the attribution of peaks at 510 and 840 cm^{-1}. For the quantitative calculation of each crystal phase, Gregorio et al. [62] used the Lambert–Beer law to determine the content of each phase in a polymorphic mixed sample, as shown in Equations (1)–(3).

$$A_\alpha = Log\frac{I_\alpha^0}{I_\alpha} = K_\alpha C X_\alpha L \quad (1)$$

$$A_\beta = Log\frac{I_\beta^0}{I_\beta} = K_\beta C X_\beta L \quad (2)$$

$$F(\beta) = \frac{X_\beta}{X_\alpha + X_\beta} = \frac{A_\beta}{(K_\beta/K_\alpha)A_\alpha + A_\beta} \quad (3)$$

where A_α and A_β represent the absorption intensity at 766 and 840 cm^{-1}, respectively, determined by I_0 and I. I_0 is the intensity of incident light, I is the intensity of transmitted light; L is the thickness of the sample, C is the monomer concentration, and X is the crystal degree, K is the absorption coefficient under a certain wavenumber; the values of K_α and K_β are calculated as 6.1×10^4 and 7.7×10^4 cm^2/mol using samples containing single α phase and β phase, respectively. Similarly, when the sample is a mixture of α phase and γ phase, the relative content of the two phases can be calculated using the same analysis method. A_α and A_γ represent the absorption intensity at 766 and 510 cm^{-1}, respectively, and the K_γ is 5.8×10^4 cm^2/mol [62].

DSC is also a commonly used method to analyze the melting point of materials and calculate crystallinity [24]. The melting point of the raw PVDF is around 148~177 °C [56]. Melting heat ΔH_f was determined from the melting peak area. Crystallinity can be evaluated by Equation (4) [57].

$$\Delta X_C = \frac{\Delta H_f}{\Delta H_{100}} \tag{4}$$

where ΔX_c represent the crystallinity, ΔH_{100} = 104.7 J/g is the melting heat for a complete crystalline sample of PVDF [44].

However, when using one method for characterization, interference factors such as preparation method and choice of raw materials will often cause changes in intensity and shift of peak positions, which will interfere with the judgment. Therefore, multiple characterization methods are often combined to analyze the structure of the sample scientifically and accurately.

3. PVDF-Based Piezoelectric Materials

3.1. Piezoelectricity

The ferroelectricity and piezoelectricity of PVDF are closely related to its crystal structure. The antiparallel arrangement of molecular chains in α phase and ε phase makes the unit cell have no net dipole moment. In the other three crystal types, the dipoles in the unit cell are parallel to each other and perpendicular to the molecular chain axis, the unit cell has a net electric dipole moment and can be spontaneously polarized. Among them, the β phase has highest dipole moments per chain per repeat unit (2.10 D) [17], dielectric permittivity and piezoelectric coefficient. Therefore, the content of β phase has the most obvious effect on piezoelectric properties, which is the most ideal phase structure [67,68].

The magnitude of the electric polarization P produced by the piezoelectric effect is proportional to the applied stress σ (Equation (5)).

$$P = d\sigma \tag{5}$$

The stress state of the crystal is determined by the second-order tensor, the electric polarization intensity is described by a vector. The piezoelectric strain coefficient d that is the most commonly used piezoelectric parameter is a third-order tensor. Due to the symmetry of the unit cell, the piezoelectric constant matrix of the PVDF film can be simplified as Equation (6) [38,69].

$$d_{ij} = \begin{pmatrix} 0 & 0 & 0 & 0 & d_{15} & 0 \\ 0 & 0 & 0 & d_{24} & 0 & 0 \\ d_{31} & d_{32} & d_{33} & 0 & 0 & 0 \end{pmatrix} \tag{6}$$

The subscript "i" is defined as the direction of electric field or electric displacement, "j" is defined as the direction of stress or strain (simplified subscript), "d" is the third order tensor.

3.2. Piezoelectric Properties of PVDF-Based Materials

PVDF and its copolymers including the P(VDF-TrFE) and P(VDF-CTFE) are all ferroelectric materials with piezoelectric and ferroelectric properties. We know that quartz crystal has weak piezoelectric activity, and complex production process, lead based piezoelectric ceramics such as lead zirconate titanate (PZT) are toxic and barium titanate ($BaTiO_3$) has a low Curie temperature and a complicated high-temperature sintering process [70,71]. Compared with these inorganic piezoelectric materials, organic polymer materials have obvious advantages in terms of mechanical properties, light weight, good flexibility and chemical stability, easy processing, nontoxic and biocompatibility, becoming a type of piezoelectric functional material that developed rapidly in the last two decades. However, the α phase of PVDF has the lowest molecular potential energy among all phases [72]. The untreated PVDF mainly crystallize in the form of α phase, but its piezoelectricity mainly depends on the polarity to β phase. Although PVDF has great flexibility, its piezoelectric constant is still small compared to inorganic piezoelectric materials. Therefore, increasing the content of the β phase becomes the key means to improve the piezoelectric activity of PVDF. Table 2 shows the comparison of the piezoelectric properties of PVDF and its copolymers with some inorganic materials.

Table 2. Performance comparison of PVDF and its copolymers with inorganic piezoelectric.

Materials	εr	Curie Point (°C)	g_{33} (10^{-3} Vm/N)	d (10^{-12} C/N)	k_{33}
PVDF	8–12 [73]	80	339 [74]	$d_{33} = -30$, d_{31} = 20–30 [5]	0.20 [75]
P(VDF-TrFE)	5–18 [76]	90	380	$d_{33} = -38$, d_{31} = 6–12 [77]	0.285 [78]
P(VDF-CTFE)	12 [79]	/	/	$d_{33} = -140$ [80] $d_{31} = 6$ [79]	0.39 [79]
Quartz	5 [5]	573	50.0 [74]	d_{11} = 2.0~2.3 [5]	/
ZnO	10.9 [81]	/	/	$d_{33} = 12.4 \pm 1.1$, $d_{31} = -5.0 \pm 0.1$ [81]	0.48 ± 0.05 [81]
$BaTiO_3$	1200 [74]	120	14.1 [74]	d_{33} = 149 [74]	/
PZT-4	1300 [74]	380	26.1 [74]	d_{33} = 289 [74]	0.64
α-BiB_3O_6	8.4 [82]	724	538 (g_{22}) [83]	d_{22} = 40.0 [82]	/

Several methods have been performed to improve this shortcoming of PVDF. For example, by stretching and applying electric field, the transformation from α phase to β phase can be induced. By repeated unidirectional poling at 650 MV/m for at least 40 times, pure β phase crystals for a biaxially oriented PVDF film can be achieved with high piezoelectricity ($d_{33} = -62$ pC/N) [84]. However, when high electric field polarization is applied, the preparation steps are complicated and time-consuming; when other structural units (TrFE, CTFE, or HPF) are introduced into PVDF, the copolymer will be directly converted to β phase without additional stretching [9,85]. For example, P(VDF-TrFE) polymer with TrFE units content higher than 20 mol% can completely convert the phase of PVDF into polar β phase crystal form with TTT conformation [86]; Inorganic or organic nanoparticles can also be used to compound with polymers, such as $BaTiO_3$ [87,88], TiO_2 [89], ZnO [27,90,91], MgO [92], Pd [93], graphene [94,95], clays [57,96], biomolecules [97] and other substances, the composite two-phase material has the advantages of low acoustic impedance and low dielectric constant. The mechanism is that the filler is usually a polar molecule or charged that can interact with the -CF_2- or -CH_2- groups of PVDF. Liu et al. [98] provide a chemical mapping of the interfacial coupling between the nanofiller and the polymer matrix in ferroelectric polymer nanocomposites by combining atomic force microscopy–infrared spectroscopy (AFM–IR) with first-principles calculations and phase-field simulations. It is

confirmed that the addition of ceramic fillers into a ferroelectric polymer leads to augmentation of the local conformational disorder in the vicinity of the interface, resulting in the local stabilization of the all-trans conformation on a molecular scale, as show in Figure 2. However, the higher surface activity and larger surface area of nanoparticles usually cause the poor dispersion in polymer matrix, agglomeration will occur, and the crystallinity of the polymer will decrease. For example, compared with pure PVDF, the crystallinity of the PVDF/ZnO composite film without surface modification of PVDF will drop from 54.76% to 47.73% [90]. Therefore, the filler is often surface modified and then compounded with the polymer.

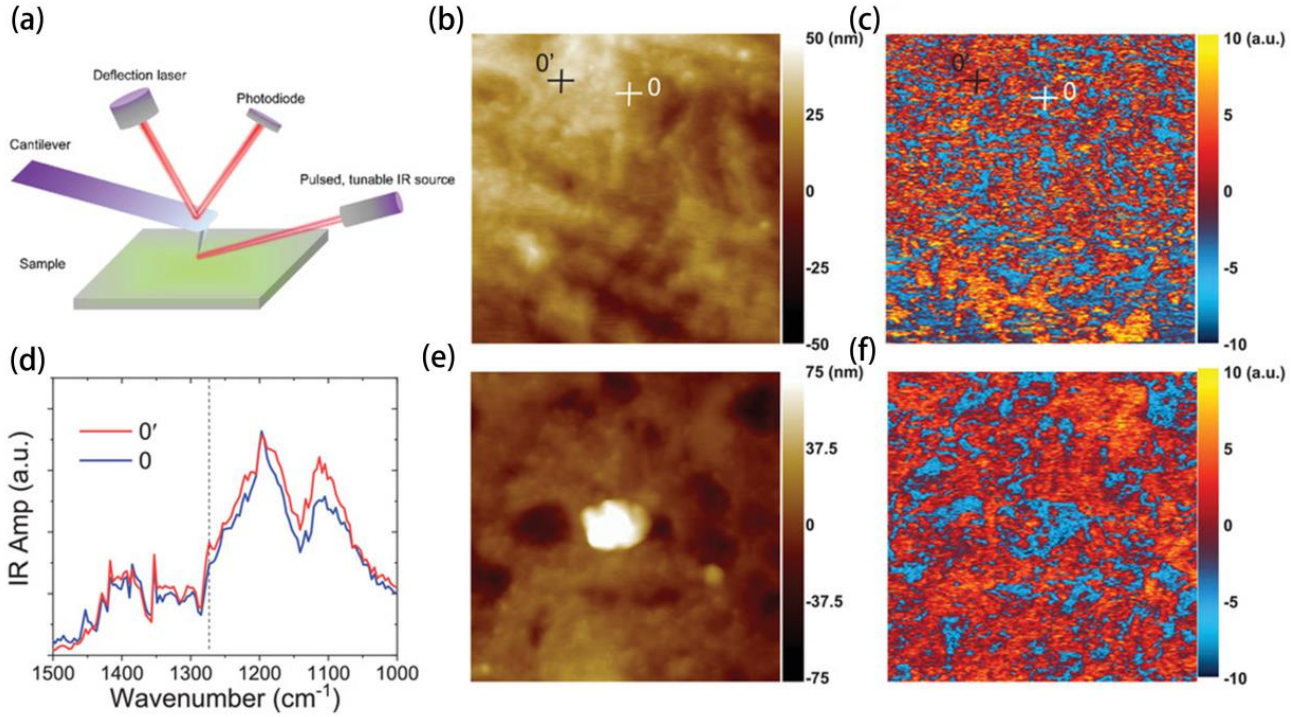

Figure 2. (**a**) Schematic of AFM–IR setup. (**b**) Simultaneously measured topography (2 × 2 μm^2) and (**c**) AFM–IR chemical maps with irradiation by a laser at 1275 cm^{-1} of P(VDF-TrFE-CFE) terpolymer. (**d**) Local spectra of the sites. (**e**) Simultaneously measured topography (2 × 2 μm^2) and (**f**) AFM–IR chemical maps with irradiation by a laser at 1275 cm^{-1} in the BTO/P(VDF-TrFE-CFE) nanocomposites with BTO of 400 nm in diameter. Reproduced from [98] with permission from the John Wiley and Sons, copyright 2020.

3.3. Fabrication Methods

Different morphologies/structures of PVDF-based materials in the forms of dense or porous films, 3D scaffolds, patterned structures, fibers and spheres can be obtained by processing technologies including doctor blade, spin coating, printing technologies, non-solvent-induced phase separation (NIPS), temperature-induced phase separation (TIPS), solvent-casting particulate leaching, solvent-casting using a 3D nylon template, freeze extraction with a 3D poly(vinyl alcohol) (PVA) template, replica molding, and electrospinning or electrospray, etc. [71].

The method of melting crystallization heats the polymer to elastomeric state and extrudes the film with uniaxial or biaxial stretching and can continuously produce the film in a large area [99], but it requires a large amount of raw materials not suitable for laboratory study to explore new functional materials. Here we introduce several commonly used methods for film preparation, solution casting [100–102], doctor blade [71], spin-coating [9,71,103–105], and inkjet printing technologies [106–109]. Solvents with stronger polarity (dimethylformamide, methyl pyrrolidone or dimethyl sulfoxide, etc.) can help the dispersion of the polymer and generation of electroactive β phase when prepare a

certain mass fraction polymer solution. String and ultrasonic dispersing can accelerate the dispersion of polymers. For solution casting method, it requires pouring the prepared solution into the mold, and a film with a certain thickness can be obtained after completely evaporating the solvent by heating. The template can be a simple petri dish for film preparation, in contrast, if 3D scaffolds are required, 3D nylon template or PVA template with different architectures and interconnected porosity have been used as templates for casting [110]. For doctor blade, with the movement of the squeegee above the substrate, the polymer solution spreads out on the substrate, the thickness of the film is controlled by polymer mass fraction and the gap size between the blade and the substrate [71]. The spin-coating method can be used to prepare even thinner films with better uniformity, but the newly formed layer will adversely influence the formerly prepared layers. After spin coating and heating, a dense film can be formed. The speed and time of spin coating, the mass fraction of the solution, and the number of spin coating layers will all affect the final thickness of the film [103]. Inkjet printing is a technology for the deposition on various substrates of high-definition patterns of different kinds of materials in a controlled and defined manner. These materials can be integrated into entirely inkjet-printed flexible electronic devices as the functional layers [106–108]. It should be noted that when preparing the P(VDF–TrFE) ink formulation, priority should be given to choose a solvent with a high boiling point and low vapor pressure to prevent the quick solvent volatilization during the printing process to form films and further block the inkjet printing [108]. Micron-level films can be obtained through multiple deposition of the ink formulation. In addition to the patterned film or electrode by inkjet printing, the photopatternable P(VDF-TrFE-CTFE) with dent azido groups can be cross-linked thermally and photochemically, such a kind of polymer has the characteristics of high dielectric constant and no need of external additives, which can be used as a negative photoresist to obtain high-quality patterned films [111]. After film preparation, annealing to reduce the residual thermal stress, and polarization to orient the dipoles should be considered.

4. Applications of PVDF-Based Piezoelectric Materials

4.1. PVDF-Based Sensors

Self-powered sensors based on flexible piezoelectric materials can respond to changes in physical quantities such as pressure [20,112–115], sound waves [116–119], temperature [94] and airflow [120], etc. The mechanical signal is directly converted into an electrical signal output. Here, several main applications of PVDF-based piezoelectric sensors are introduced.

4.1.1. Pressure Sensors

The PVDF-based piezoelectric materials are explored for pressure sensors, which have been used in various fields such as engineering, physiological testing and micro-mechanical elements. The state of the polymer is mainly thin film or nanofiber. The overall structure is mostly a sandwich structure, where the upper and lower layers are electrodes, and the middle layer is PVDF-based piezoelectric materials. Through the detected pressure change, the pressure sensor can be used to detect whether the pipeline valve is normally switched [112]. As the charge generated on the electrodes by straining the foil is discharging slowly, the sensor is suitable for the detection of dynamic low-frequency pressure changes. It has the advantages of good aging resistance at low temperatures and low pressures, low production cost, short response time, and wide operating temperature and pressure ranges, but the measurement accuracy is limited by the intersection of temperature, thermoelectricity and temperature sensitivity. In addition, the P(VDF-TrFE) copolymer can be obtained by spin-coating on the silicon substrate into thin film (1 μm). A thin film sensor with a metal-P(VDF-TrFE)-metal structure, which can achieve rapid recovery, was fabricated by a lithography process. Due to its compact form factor and biocompatibility, it can be integrated with catheters to detect blood flow direction and vascular pressure, making it a huge application potential in the field of implantable medical

devices [20]. As shown in Figure 3a,b, the highly oriented P(VDF-TrFE) nanofibers prepared by electrospinning technology have high sensitivity, and the simple pressure sensor shows excellent response in a wide pressure range. The sensitivity is found to be 1.1 V/kPa within the pressure range of 0.4~2 kPa [21]. In addition to applying positive pressure to cause the material to bend and deform to produce piezoelectric response, PVDF can also be designed as a simple accelerometer, vibrometer, and orientation sensors, promising for uses in self-balancing robots and sensitive impact detectors.

PVDF-based pressure sensors also show a wide range of applications in the field of wearable devices for human–computer interaction. The skin-interactive metal-free spongy electrode in a piezoelectric sensor where highly aligned poly(vinylidene fluoride) (PVDF) nanofiber (NF) arrays are introduced as the piezoelectric active component and conducting polyaniline- (PANI-) coated PVDF (PANI−PVDF) NFs mats served as flexible electrodes (Figure 3c), this design effectively avoids the disadvantages of poor compatibility and fragility of metal electrodes, at the same time, shows excellent mechanical to electrical energy conversion property (Figure 3d) that enables to sense human finger touch with a high energy conversion efficiency being in the order of 53% [22]. Due to the piezoelectric and pyroelectric effects of PVDF, electrospinning nanofibers are also used to manufacture highly sensitive wearable pressure sensors and pyroelectric respiration sensors. The graphene doped PVDF materials are found to show better performances (Figure 3e) [94]. Such pressure sensors exhibit high sensitivity to the bending and stretching of fingers, wrists and elbows, and can detect a variety of human physiological signals (Figure 3f). In addition to graphene, the molecular ferroelectric (dabcoHReO$_4$, DH) is also used to compound with PVDF, and the hydrogen bond between them can be utilized to prepare a composite film with a high β crystal form content (95%), which can be applied for flexible electronic sensing equipment with excellent performance [114]. Core/shell PVDF/dopamine (DA) nanofibers with a very high β crystal form content (93%) and self-aligned polarization can be fabricated by electrospinning (Figure 3g), the all-fiber-based soft sensor fabricated and tested on human skin and in vivo in mice shows a high sensitivity and accuracy for detecting weak physiological mechanical stimulation from diaphragm motions and blood pulsation [97].

In addition to modifying the material itself, the patterned electrode can also effectively improve the sensitivity of the device [34,121,122]. A pair of dislocation interdigital electrodes are designed on the upper and lower surfaces of the P(VDF-TrFE) piezoelectric film by inkjet printing (Figure 3h). Then, by applying a high voltage, multiple alternating oblique polarization regions (Figure 3i,j) are generated inside the cross-sectional area, which exhibits enhanced sensitivity to an external stress stimulation [34].

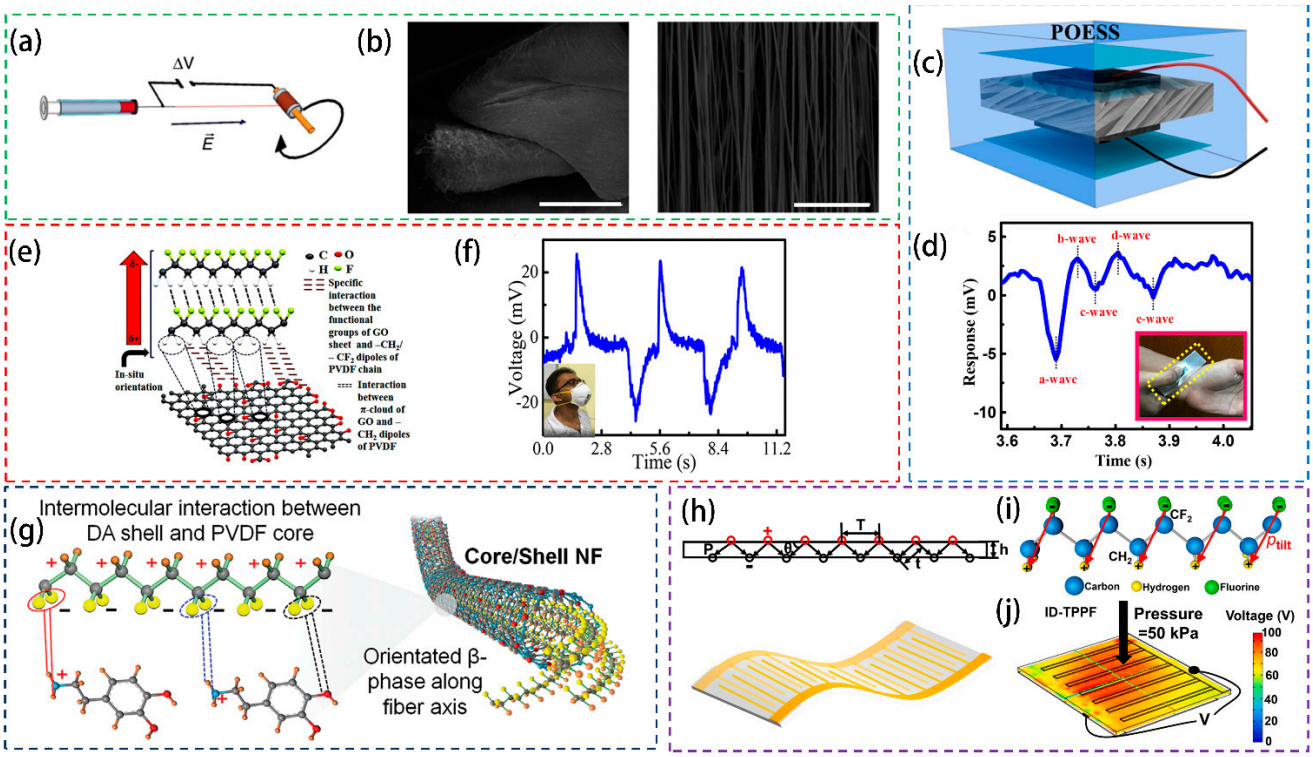

Figure 3. (**a**) Schematic illustration of the experimental setup for electrospinning highly aligned arrays of oriented nanofibers of aligned polymer chains of P(VDF-TrFE). (**b**) Photograph of a free-standing film of highly aligned piezoelectric fibers, SEM micrograph of fibers arrays. Reproduced from [21] with permission from the Springer Nature, copyright 2013. (**c**) Three dimensional schematic illustrations of piezo-organic e-skin sensor (POESS) design architecture. (**d**) Radial artery pulse measurement response by simply interfacing the POESS to the human wrist. Reproduced from [22] with permission from the American Chemical Society, copyright 2020. (**e**) Schematic of a hypothetical model for electroactive phase nucleation and interactions present in PVDF/1 wt% GO nanofibers. (**f**) Open circuit voltage of thePVDF/1wt % GO-based nanogenerator devices (photo of the deviceattached to a N95 breathing mask is shown in the inset) driven by human respiration at room temperature. Reproduced from [94] with permission from the American Chemical Society, copyright 2019. (**g**) A Schematic of the Core/shell PVDF/DA nanofibers. Reproduced from [97] with permission from the John Wiley and Sons, copyright 2020. (**h**) Schematic illustration of alternatively tilt-polarized P(VDF-TrFE) film. (**i**) Molecular chain arrangement and tilt dipole orientation p_{tilt} of P(VDF-TrFE) polymer. (**j**) The voltage distribution on ID-TPPF under a dynamic pressure of 50 kPa. Reproduced from [34] with permission from Elsevier, copyright 2021.

4.1.2. Acoustic Sensors

Sound detection and recognition sensors (SDRs) based on electrostatic, capacitive, electromagnetic or electrical methods have the disadvantages of large size, internal power supply and low electro-acoustic conversion efficiency. In contrast, the PVDF-based piezoelectric sensor has the characteristics of small size, flexibility, self-powered, high acoustic-electric conversion efficiency and high signal-to-noise ratio, which can meet the current requirements for SDRs applications [116].

Piezoelectric acoustic sensors require the sensing materials to possess the merits of good flexibility and high sensitivity. Electrospinning technology is a feasible method to fabricate PVDF nanofibers, which are easy to vibrate under sound waves. The PVDF piezoelectric nanofiber sensors prepared by electrospinning can distinguish sound waves of different frequencies even similar frequencies. Figure 4a shows the entire workflow of the sensor, and Figure 4b illustrates the proposed sound sensing mechanism [118]. As can be observed, such kind of device shows high sensitivity to sounds above 100 decibels. It is worth mentioning that there is a maximum voltage output when sound frequency is 220 Hz (Figure 4c), which can be used for noise detection. In addition to the traditional resonant system sensor, a suspended, transparent, nonresonant acoustic sensor is prepared through

the dynamic near-field electrospinning (dNFES) process, which has a wide frequency response range, high resolution and high fidelity, and can be applied for voice recognition and recording [123]. When the individual nanofibers vibrate under the acoustic field in a collective manner, an output voltage is generated (Figure 4d). The sensing device can detect acoustic signals in the frequency range of 200~5000 Hz (Figure 4e) which covers the most common audible sound frequency spectrum in daily life. Particularly, the PVDF based SDRs can differentiate two similar input sound frequencies (Figure 4f). Meanwhile, due to the high transparency and high permeability of the nanofiber network, it can be combined with optical and gas sensors to collect multidimensional information in the same smart device platform. Of course, traditional membranes can also be used as acoustic sensors. Ionic liquid in-situ electric field polarization can be used to obtain flexible, accurate and highly sensitive P(VDF-TrFE) film (Figure 4g) [116]. Sensors based on the film can identify and distinguish complex sound signals, such as those musical notes of different frequencies (Figure 4h), bass and treble (Figure 4i), and the frequencies produced by different species that have great potential in various applications such as microphones, biometrics, environmental protection, and artificial intelligence.

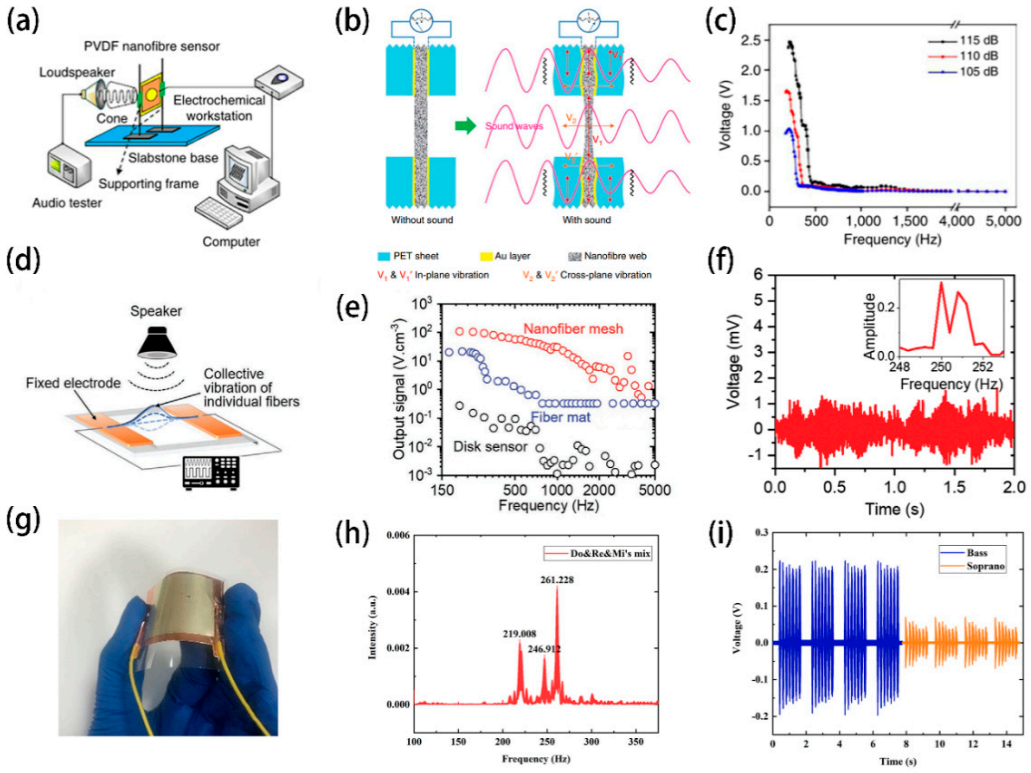

Figure 4. Schematic illustration of (**a**) the setup for testing the device, (**b**) proposed sound vibration modes and piezoelectric conversion mechanism for the nanofiber device. (**c**) The effect of sound wave frequency on output voltage. (**d**) Schematic illustration of the experimental setup. Reproduced from [118] with permission from the Springer Nature, copyright 2016. (**e**) Acoustic sensing bandwidth of the nanofiber mesh compared with the 40 μ m thick nanofiber mat and a commercial piezoelectric acoustic sensing dish. (**f**) Signal output of nanofiber mesh at two interfering frequencies (250, 251 Hz) at 70 dB, and the FFT processed spectrum. Reproduced from [123] with permission from the John Wiley and Sons, copyright 2020. (**g**) The photo of SDRS. (**h**) Frequency domain signal map as detected by the SDRS from a sound signal consisting of mixed Do, Re and Mi tones. (**i**) Voltage signal diagram of the bass and soprano sound collected by the device. Reproduced from [116] with permission from the Elsevier, copyright 2020.

Nondestructive testing is often used for performing process monitoring (PM) and structural health monitoring (SHM) to assess the quality of the produced composite parts [124]. For the external nondestructive testing, such as radiographic testing, electromagnetic (EM) testing, acoustic emission (AE) testing, infrared thermography (IRT)

testing, etc., they have to be instrumented on the surface or even out of the parts, and are done in a particular period inconstantly, in-situ SHM techniques can do continuous monitoring of the structure and can reduce the environmental interference due to the encapsulation [124,125]. PVDF devices have also been used as in-situ acoustic emission sensors [126–128]. Damage sensing and interfacial evaluation of single-glass or basalt fibers/epoxy composites can be monitored through AE [128]. Due to the limited sensitivity compared with PZT, only fiber fracture signals can be detected by the piezoelectric PVDF sensor with 30μm glass composite without matrix crack and interfacial debonding signals. The advantage of the PVDF is that it is diverse in the choice of contacting methods, piezoelectric PVDF sensors can be attached or embedded in the composite to monitor the composites without sensitivity loss contributed from their ductile flexibility. De Rosa et al. [127] performed an investigation based on AE with PVDF sensors as AE sensors, which are surface-mounted and embedded in glass/epoxy laminates. The sensors are used to monitor the laminates while being subjected to tension, three-point bending and post-impact three-point bending. Table 3 shows the performances of several kinds of PVDF-based piezoelectric sensors which are mentioned.

Table 3. Performances of several kinds of PVDF-based piezoelectric sensors.

Materials	Preparation Methods	Size	Testing Conditions	Sensitivity (V/kpa)	Detection Capability	Output Voltage (V)
P(VDF–TrFE) [21]	Electrospinning	/	Dynamic bending	/	0.1 Pa	1.5
PVDF [22]	Electrospinning	6 × 3 cm^2	Dynamic pressure 10 kPa, 1~5 Hz	0.8	/	10
PVDF/GO [94]	Electrospinning	2.5 × 5 cm^2	Static and dynamic	4.3	10 Pa	/
PVDF/DH [114]	Solution coating	50 μm thick	Dynamic force (6 N, 8 Hz)	/	/	3.2
PVDF/DA [97]	Electrospinning	2 × 1 cm^2, 30 μm thick	Dynamic pressure (1 kPa, 1.2 Hz)	/	/	16
P(VDF–TrFE) [34]	Inkjet printing	3.2 × 1 cm^2, 150 μm thick	Dynamic pressure (50 kPa, 1 Hz)	1.47	0.3~50 kPa	73.5
PVDF [118]	Electrospinning	40 μm thick	Sound waves (220 Hz, 115 dB)	0.266	<2000 Hz	3.10
P(VDF–TrFE) [123]	Electrospinning	0.3 × 6 cm^2, 307 nm thick	Sound waves (250 Hz, 95 dB)	/	200~5000 Hz	0.2
P(VDF–TrFE) [116]	Screen coating	10 μm thick	Sound waves	/	20~20 kHz	~700 μ

4.2. PVDF Nanogenerators

In 2006, Professor Zhonglin Wang proposed the use of ZnO nanowire (NW) arrays to convert micro-nano mechanical energy into electrical energy, that is, the strategy of nanogenerators [129]. In addition to the usage as a self-powered sensor, nanogenerators can provide electrical energy for micro-nano electronic devices and can also directly provide electrical energy for chemical reactions [26]. PVDF nanogenerators can collect mechanical energy from the environment [29,130,131] or human movement [28,132–134] and convert it into electrical energy. Compared with traditional rigid and fragile piezoelectric ceramics, the flexible PVDF electronic devices are becoming a current research focus due to their excellent flexibility and easy processing technology.

According to the piezoelectric mechanism, when suffering from the dynamics of non-zero strain rate, the positive and negative charge centers will separate, which leads to polarization and changes in bound charge. The flow of free charge in the drive circuit is used to shield the bound charge, generating alternating current, and the net charge continuously generates voltage across the nanogenerator. Pi et al. [9] used spin-coating method to prepare P(VDF-TrFE) film on polyimide (PI) substrate as the functional layer of the nanogenerator (Figure 5a), and the short-circuit current and open-circuit voltage changes of the nanogenerator in the cyclic stretching-releasing process are explained through experiments and models (Figure 5b).

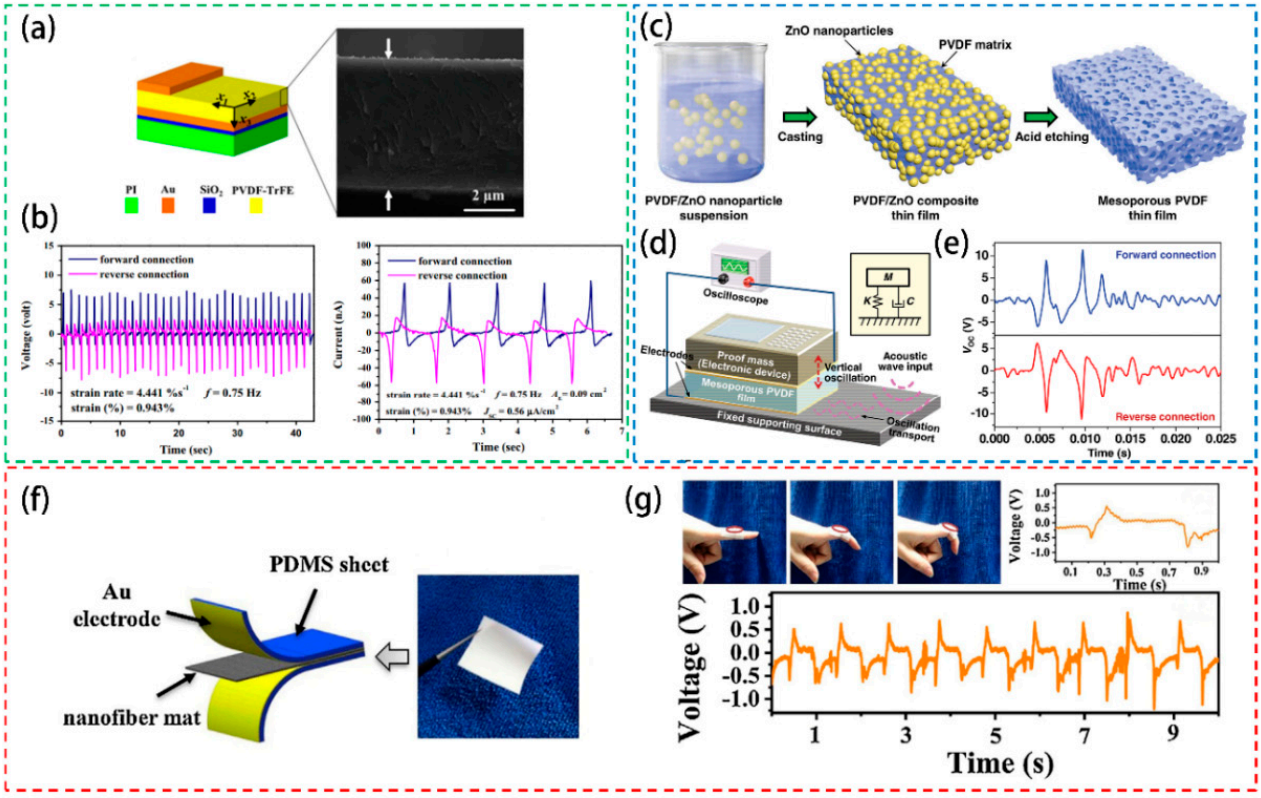

Figure 5. (**a**) Schematic illustration of P(VDF-TrFE) thin film-based NG and cross-sectional SEM image of the 6.5 μm thick copolymer film. (**b**) The open-circuit voltage and short-circuit current of a piezoelectric thin film-based NG subject to loading frequency f = 0.75 Hz and strain magnitude 0.943%. Reproduced from [9] with permission from the Elsevier, copyright 2014. (**c**) Schematic procedure for fabricating mesoporous piezoelectric PVDF thin films. (**d**) Schematic setup for characterizing PVDF thin film NGs for harvesting mechanical energy from surface oscillations. The mesoporous PVDF thin film-weight system can be simplified as a free vibration system with damping, as shown in the inset. (**e**) The voltage output of a PVDF thin film NG (fabricated from a 50% ZnO mass fraction mixture) generated during one cycle of surface oscillation. The blue and red curves were collected under forward and reverse connections. Reproduced from [26] with permission from the John Wiley and Sons, copyright 2014. (**f**) The schematic illustration of BZT-BCT/P(VDF-TrFE) nanogenerator and the photo of the nanofiber mats. (**g**) The output voltage from the generator with 40 wt% BZT-BCT content attached on the finger joint. Reproduced from [135] with permission from the Elsevier, copyright 2021.

As mentioned in part three, the piezoelectric performance of the doped PVDF film will be improved when comparing to the pure PVDF. Mao et al. [26] obtained PVDF/ZnO composite film by solution casting, and then etched ZnO with hydrochloric acid solution to obtain mesoporous PVDF film (Figure 5c). This fabrication method circumvents the requirement of large mechanical strain or high electric field for the formation of β phase PVDF, and using the electronic device's own weight to modulate its displacement and amplify its electrical output realizes a very simple system design (Figure 5d,e). This simple-designed device is easy to integrate into other systems and is used in self-powered

electronic equipment. Recently, the lead-free piezoelectric ceramics were also used to compound with PVDF for use in wearable or implantable devices. The flexible composite film doped with $0.5Ba(Zr_{0.2}Ti_{0.8})O_3$-$0.5(Ba_{0.7}Ca_{0.3})TiO_3$ (BZT-BCT) can be prepared by the electrospinning (Figure 5f), which exhibits excellent voltage output performance, the output voltage as high as 13.01 V under cyclic tapping under 6 N at 10 Hz [135]. Besides, nanogenerator can respond to the activities of the human body to show their applications in wearable field (Figure 5g). Jella et al. [136] compounded methylammonium lead iodide ($MAPbI_3$) perovskite with PVDF and compared the output performance of the composite films with different thicknesses (36.9, 69.3 and 97.7 μm). It is reported that the composites with higher thickness exhibited more outstanding piezoelectric output performance than the thinner ones. Results show that the output voltage value and other parameters are closely related to the thickness of the electroactive layer. In addition to the inorganic materials, researchers have gradually turned their visions to the combination of PVDF-based materials with other organic materials for seeking the improved performance of the nanogenerators and meanwhile achieving better biocompatibility and degradability, for example, the biowaste crab shell-extracted chitin nanofiber (CFN) [137] and vitamin B_2 [29]. Table 4 shows the performances of PVDF-based piezoelectric nanogenerators

Table 4. Performances of several kinds of PVDF-based piezoelectric nanogenerators.

Materials	Preparation Methods	Size	Testing Conditions	Output Voltage (V)	Output Current (Power)	Output Current (Power) Density
P(VDF–TrFE) [9]	Spin coating	0.09 cm^2, 6.5 μm thick	Stretching–releasing cycle	7	0.058 μA	0.56 μA/cm^2
PVDF/ZnO [26]	Casting-etching	2 × 1 cm^2, 28 μm thick	Oscillating at 40 Hz	11.0	9.8 μA	/
PVDF/BZT-BCT [135]	Electrospinning	1 cm^2(eff), 40 μm thick	Dynamic force (6 N, 10 Hz)	13.01	1.44 μW	/
PVDF/$MAPbI_3$ [136]	Drop casting	3 × 3 cm^2, 97.7 μm thick	Dynamic force (50 N, 5 Hz)	45.6	/	4.7 μA/cm^2
PVDF/CNF [137]	Solution casting	2.4 × 1.5 cm^2, 90 μm thick	Finger impartation (25 kPa, 6 Hz)	49	1.9 μA	6.6 mW/m^3
PVDF/VB_2 [29]	Spin coating	1.0 × 1.6 cm^2	Dynamic force (80 N, 3 Hz)	61.5 V	12.2 μA	9.3 mW/m^3

4.3. Biomedical Applications

Taking the advantage of biocompatible feature, the PVDF-based piezoelectric polymer is explored for biomedical applications. The PVDF based materials can be used for simulating the extracellular matrix environment and use in vivo physiological activities or environmental stimuli to generate in-situ electrical signals to promote bone [138,139], nerves [30,32] and muscle [33] regeneration as well as biological tissue engineering.

Genchi et al. [32] prepared a P(VDF-TrFE)/$BaTiO_3$ nanoparticle composite film (Figure 6a), which presents better piezoelectric properties than the pure P(VDF-TrFE) and can support the proliferation and differentiation of SH-SY5Y cells. What is more, the piezoelectricity of the film can be activated under ultrasound stimulation, so that the number of β3-tubulin-positive cells and the axon length of the cells on the P(VDF-TrFE)/BTNP composite film could be increased significantly (Figure 6b), thus, the film can be applied for use as wireless neuron stimulation devices. For the selection of piezoelectric materials, $BaTiO_3$ nanoparticles and P(VDF-TrFE) composite were applied [140], and polydopamine was introduced on

BTO nanoparticles to achieve better interface compatibility between BTO nanoparticles and P(VDF-TrFE), as shown in Figure 6c. Solution casting method is chosen to prepare composite film and then conduct polarization treatment. It is reported that the material promotes the in vitro osteogenic behavior of bone marrow mesenchymal stem cells. Furthermore, it can also promote the continuous maintenance of the in vivo electrical microenvironment, rapid and extensive healing of bone defects (Figure 6d).

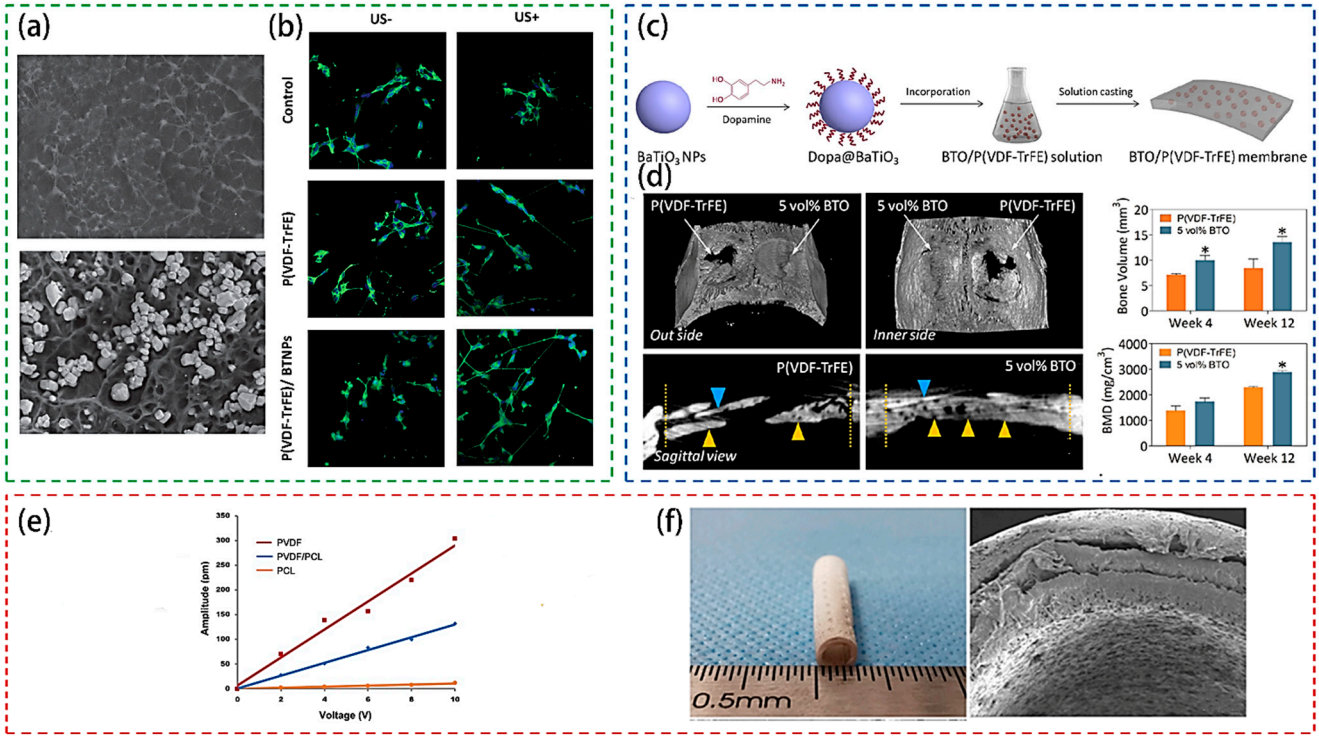

Figure 6. (**a**) Scanning electron microscopy images of P(VDF-TrFE) films and P(VDF-TrFE)/BTNP films. (**b**) Confocal fluorescence microscopy images of SH-SY5Y neuroblastoma cells at the end of a differentiation period of 6 days on P(VDF-TrFE), P(VDF-TrFE)/BTNP films, and on Ibidi film as control. Cells were either unexposed or exposed to chronic US stimulation. Reproduced from [32] with permission from the John Wiley and Sons, copyright 2016. (**c**) Schematic illustration of the preparation process of BTO/P(VDF-TrFE) membrane. (**d**) Bone defect repair in rat calvarial models after implantation of polarized nanomembranes with 5 vol% BTO content and polarized neat P(VDF-TrFE) membranes. Reproduced from [140] with permission from the American Chemical Society, copyright 2016. (**e**) Piezoelectric response of PVDF, 20% PVDF/PCL, PCL, in terms of the average values of amplitude responded to applied a.c. voltage. (**f**) SEM images of the multilayered and microporous structure for 20% PVDF/PCL scaffolds. Reproduced from [30] with permission from the Elsevier, copyright 2020.

Damaraju et al. [31] used electrospinning to prepare three-dimensional fiber scaffolds to stimulate the differentiation and tissue formation of mesenchymal stem cells (MSC). Cheng et al. [30] used the casting/annealing-solvent replacement method to composite the degradable material polycaprolactone (PCL) and PVDF to prepare a porous nerve tissue engineering scaffold (Figure 6f). Compared with a scaffold with a high elastic modulus prepared by electrospinning, such a design shows strong mechanical strength. In addition, the stent exhibits better biodegradability and biocompatibility, which can avoid the process of removing the implant material in the second operation. This kind of composite scaffold can achieve the function of promoting regeneration and recovery of a 15 mm rat with sciatic nerve defect. Figure 6e gives the average piezoelectric response amplitude induced by applied a.c. voltage. The slope of the piezoelectric response amplitude versus the applied voltage for PVDF/PCL scaffolds is dramatically increased. It needs to be pointed out that when exploring PVDF piezoelectric materials for biomedicine applications, more factors should be taken into account, such as biocompatibility and mechanical properties, etc.

5. Summary and Outlook

PVDF based piezoelectric materials have shown more and more application potentials in sensors, power generation and biomedicine, etc., due to their excellent physical and mechanical properties, chemical stability, and low production costs. Besides, the combination of piezoelectric properties with other properties such as acoustics, optics, and thermals to design multifunctional integrated systems is also becoming an important direction of the current research.

At present, there are many methods for preparing PVDF based polymer films, but pure PVDF requires stretching and polarization post-processing operations, and the process is complicated. Therefore, the improvment of the preparation process and the piezoelectric performance is one of the follow-up studies. In addition, research on composite piezoelectric materials based on PVDF materials is active. Exploring new composite films using materials with strong piezoelectric activity would improve the properties of the PVDF based composites. Choosing appropriate inorganic or organic materials to construct new structures will be more conducive to improving the corresponding level of piezoelectricity of the film and the applicable scope of the related device.

PVDF has a complex conformation, and the crystalline region and the amorphous region coexist, hence, the crystallization mechanism is complex. Though many studies to date focus on the design and application of related devices, the fundamental and deep studies on the intrinsic properties of PVDF materials are limited. How the transformation occurs between different conformations, which component is primarily responsible for the piezoelectricity, and how the composite films improve piezoelectric performance are worth further investigation. What is more, although the performance and application of PVDF-based materials have made important progress in laboratory stage, they still face many challenges for industrial applications, and some questions about the fatigue and the durability after composition need further investigations.

Author Contributions: L.X. and G.W. contributed equally to this work. Conceptualization, L.X., G.W. and F.Y.; methodology, G.W.; software, C.J.; writing—original draft preparation, L.X. and G.W.; writing—review and editing, F.Y. and X.Z.; project administration, F.Y. and X.Z. All authors have read and agreed to the published version of the manuscript.

Funding: This research was funded by [the National Natural Science Foundation of China] grant number [51872165], [the Primary Research & Development Plan of Shandong Province] grant number [2019JZZY010313] and [Shandong Provincial Natural Science Foundation] grant number [ZR2020KA003].

Institutional Review Board Statement: Not applicable.

Informed Consent Statement: Not applicable.

Data Availability Statement: Not applicable.

Conflicts of Interest: The authors declare no conflict of interest.

References

1. Mason, W.P. Piezoelectricity, its history and applications. *J. Acoust. Soc. Am.* **1981**, *70*, 1561–1566. [CrossRef]
2. Mathur, S.C.; Scheinbeim, J.I.; Newman, B.A. Piezoelectric properties and ferroelectric hysteresis effects in uniaxially stretched nylon-11 films. *J. Appl. Phys.* **1984**, *56*, 2419–2425. [CrossRef]
3. Huang, L.; Zhuang, X.; Hu, J.; Lang, L.; Zhang, P.; Wang, Y.; Chen, X.; Wei, Y.; Jing, X. Synthesis of Biodegradable and Electroactive Multiblock Polylactide and Aniline Pentamer Copolymer for Tissue Engineering Applications. *Biomacromolecules* **2008**, *9*, 850–858. [CrossRef] [PubMed]
4. Buchberger, G.; Schwödiauer, R.; Bauer, S. Flexible large area ferroelectret sensors for location sensitive touchpads. *Appl. Phys. Lett.* **2008**, *92*, 123511. [CrossRef]
5. Lovinger, A.J. Ferroelectric Polymers. *Science* **1983**, *220*, 1115–1121. [CrossRef] [PubMed]
6. Martins, P.; Lopes, A.C.; Lanceros-Mendez, S. Electroactive phases of poly(vinylidene fluoride): Determination, processing and applications. *Prog. Polym. Sci.* **2014**, *39*, 683–706. [CrossRef]
7. Ueberschlag, P. PVDF piezoelectric polymer. *Sens. Rev.* **2001**, *21*, 118–126. [CrossRef]

8. Mohammadi, B.; Yousefi, A.A.; Bellah, S.M. Effect of tensile strain rate and elongation on crystalline structure and piezoelectric properties of PVDF thin films. *Polym. Test.* **2007**, *26*, 42–50. [CrossRef]
9. Pi, Z.; Zhang, J.; Wen, C.; Zhang, Z.-B.; Wu, D. Flexible piezoelectric nanogenerator made of poly(vinylidenefluoride-co-trifluoroethylene) (PVDF-TrFE) thin film. *Nano Energy* **2014**, *7*, 33–41. [CrossRef]
10. Wan, C.; Bowen, C.R. Multiscale-structuring of polyvinylidene fluoride for energy harvesting: The impact of molecular-, micro- and macro-structure. *J. Mater. Chem. A* **2017**, *5*, 3091–3128. [CrossRef]
11. Liu, Y.; Wang, Q. Ferroelectric Polymers Exhibiting Negative Longitudinal Piezoelectric Coefficient: Progress and Prospects. *Adv. Sci.* **2020**, *7*, 1902468. [CrossRef]
12. Kawai, H. The Piezoelectricity of Poly (vinylidene Fluoride). *Japanese J. Appl. Phys.* **1969**, *8*, 975–976. [CrossRef]
13. Kepler, G.R. Piezoelectricity, Pyroelectricity, and Ferroelectricity in Organic Materials. *Ann. Rev. Phys. Chem.* **1978**, *29*, 497–518. [CrossRef]
14. Tamura, M.; Ogasawara, K.; Ono, N.; Hagiwara, S. Piezoelectricity in uniaxially stretched poly(vinylidene fluoride). *J. Appl. Phys.* **1974**, *45*, 3768–3771. [CrossRef]
15. Park, C.; Lee, K.; Koo, M.; Park, C. Soft Ferroelectrics Enabling High-Performance Intelligent Photo Electronics. *Adv. Mater.* **2020**, e2004999. [CrossRef]
16. Broadhurst, M.G.; Davis, G.T.; McKinney, J.E.; Collins, R.E. Piezoelectricity and pyroelectricity in polyvinylidene fluoride—A model. *J. Appl. Phys.* **1978**, *49*, 4992–4997. [CrossRef]
17. Soulestin, T.; Ladmiral, V.; Dos Santos, F.D.; Améduri, B. Vinylidene fluoride- and trifluoroethylene-containing fluorinated electroactive copolymers. How does chemistry impact properties? *Prog. Polym. Sci.* **2017**, *72*, 16–60. [CrossRef]
18. Ambrosy, A.; Holdik, K. Piezoelectric PVDF films as ultrasonic transducers. *J. Phys. E Sci. Instrum.* **1984**, *17*, 856–859. [CrossRef]
19. Sharma, T.; Aroom, K.; Naik, S.; Gill, B.; Zhang, J.X.J. Flexible Thin-Film PVDF-TrFE Based Pressure Sensor for Smart Catheter Applications. *Ann. Biomed. Eng.* **2012**, *41*, 744–751. [CrossRef]
20. Sharma, T.; Je, S.-S.; Gill, B.; Zhang, J.X. Patterning piezoelectric thin film PVDF–TrFE based pressure sensor for catheter application. *Sens. Actuators A Phys.* **2012**, *177*, 87–92. [CrossRef]
21. Persano, L.; Dagdeviren, C.; Su, Y.; Zhang, Y.; Girardo, S.; Pisignano, D.; Huang, Y.; Rogers, J.A. High performance piezoelectric devices based on aligned arrays of nanofibers of poly(vinylidenefluoride-co-trifluoroethylene). *Nat. Commun.* **2013**, *4*, 1633. [CrossRef]
22. Maity, K.; Garain, S.; Henkel, K.; Schmeißer, D.; Mandal, D. Self-Powered Human-Health Monitoring through Aligned PVDF Nanofibers Interfaced Skin-Interactive Piezoelectric Sensor. *ACS Appl. Polym. Mater.* **2020**, *2*, 862–878. [CrossRef]
23. Zhou, Z.; Du, X.; Luo, J.; Yao, L.; Zhang, Z.; Yang, H.; Zhang, Q. Coupling of interface effects and porous microstructures in translucent piezoelectric composites for enhanced energy harvesting and sensing. *Nano Energy* **2021**, *84*, 105895. [CrossRef]
24. Naik, R.N.; Rao, T.S. Self-powered flexible piezoelectric nanogenerator made of poly (vinylidene fluoride)/Zirconium oxide nanocomposite. *Mater. Res. Express* **2019**, *6*, 115330. [CrossRef]
25. Lu, L.; Ding, W.; Liu, J.; Yang, B. Flexible PVDF based piezoelectric nanogenerators. *Nano Energy* **2020**, *78*, 105251. [CrossRef]
26. Mao, Y.; Zhao, P.; McConohy, G.; Yang, H.; Tong, Y.; Wang, X. Sponge-Like Piezoelectric Polymer Films for Scalable and Integratable Nanogenerators and Self-Powered Electronic Systems. *Adv. Energy Mater.* **2014**, *4*, 4. [CrossRef]
27. Sahoo, R.; Mishra, S.; Ramadoss, A.; Mohanty, S.; Mahapatra, S.; Nayak, S.K. An approach towards the fabrication of energy harvesting device using Ca-doped ZnO/ PVDF-TrFE composite film. *Polymer* **2020**, *205*, 122869. [CrossRef]
28. Siddiqui, S.; Kim, D.-I.; Duy, L.T.; Nguyen, M.T.; Muhammad, S.; Yoon, W.-S.; Lee, N.-E. High-performance flexible lead-free nanocomposite piezoelectric nanogenerator for biomechanical energy harvesting and storage. *Nano Energy* **2015**, *15*, 177–185. [CrossRef]
29. Karan, S.K.; Maiti, S.; Agrawal, A.K.; Das, A.K.; Maitra, A.; Paria, S.; Bera, A.; Bera, R.; Halder, L.; Mishra, A.K.; et al. Designing high energy conversion efficient bio-inspired vitamin assisted single-structured based self-powered piezoelectric/wind/acoustic multi-energy harvester with remarkable power density. *Nano Energy* **2019**, *59*, 169–183. [CrossRef]
30. Cheng, Y.; Xu, Y.; Qian, Y.; Chen, X.; Ouyang, Y.; Yuan, W.-E. 3D structured self-powered PVDF/PCL scaffolds for peripheral nerve regeneration. *Nano Energy* **2020**, *69*, 104411. [CrossRef]
31. Damaraju, S.M.; Shen, Y.; Elele, E.; Khusid, B.; Eshghinejad, A.; Li, J.; Jaffe, M.; Arinzeh, T.L. Three-dimensional piezoelectric fibrous scaffolds selectively promote mesenchymal stem cell differentiation. *Biomaterials* **2017**, *149*, 51–62. [CrossRef]
32. Genchi, G.G.; Ceseracciu, L.; Marino, A.; Labardi, M.; Marras, S.; Pignatelli, F.; Bruschini, L.; Mattoli, V.; Ciofani, G. P(VDF-TrFE)/$BaTiO_3$ Nanoparticle Composite Films Mediate Piezoelectric Stimulation and Promote Differentiation of SH-SY5Y Neuroblastoma Cells. *Adv. Health Mater.* **2016**, *5*, 1808–1820. [CrossRef]
33. Martins, P.; Ribeiro, S.; Sencadas, V.; Gomes, A.C.; Gama, F.M.; Lanceros-Méndez, S. Effect of poling state and morphology of piezoelectric poly(vinylidene fluoride) membranes for skeletal muscle tissue engineering. *RSC Adv.* **2013**, *3*, 17938–17944. [CrossRef]
34. Yuan, X.; Gao, X.; Shen, X.; Yang, J.; Li, Z.; Dong, S. A 3D-printed, alternatively tilt-polarized PVDF-TrFE polymer with enhanced piezoelectric effect for self-powered sensor application. *Nano Energy* **2021**, *85*, 105985. [CrossRef]
35. Shi, L.; Jin, H.; Dong, S.; Huang, S.; Kuang, H.; Xu, H.; Chen, J.; Xuan, W.; Zhang, S.; Li, S.; et al. High-performance triboelectric nanogenerator based on electrospun PVDF-graphene nanosheet composite nanofibers for energy harvesting. *Nano Energy* **2021**, *80*, 105599. [CrossRef]

36. Li, Y.; Zhao, Z.; Liu, L.; Zhou, L.; Liu, D.; Li, S.; Chen, S.; Dai, Y.; Wang, J.; Wang, Z.L. Improved Output Performance of Triboelectric Nanogenerator by Fast Accumulation Process of Surface Charges. *Adv. Energy Mater.* **2021**, *11*, 2100050. [CrossRef]
37. Li, Y.; Zhou, B.; Shen, Y.; He, C.; Wang, B.; Liu, C.; Feng, Y.; Shen, C. Scalable manufacturing of flexible, durable Ti3C2Tx MXene/Polyvinylidene fluoride film for multifunctional electromagnetic interference shielding and electro/photo-thermal conversion applications. *Compos. Part B Eng.* **2021**, *217*, 108902. [CrossRef]
38. Lovinger, A.J. Poly(Vinylidene Fluoride). In *Developments in Crystalline Polymers—1*; Bassett, D.C., Ed.; Springer: Berlin, Germany, 1982; pp. 195–273.
39. Hasegawa, R.; Takahashi, Y.; Chatani, Y.; Tadokoro, H. Crystal Structures of Three Crystalline Forms of Poly(vinylidene fluoride). *Polym. J.* **1972**, *3*, 600–610. [CrossRef]
40. Bachmann, M.; Gordon, W.L.; Weinhold, S.; Lando, J.B. The crystal structure of phase IV of poly(vinylidene fluoride). *J. Appl. Phys.* **1980**, *51*, 5095–5099. [CrossRef]
41. Takahashi, Y.; Tadokoro, H. Crystal Structure of Form III of Poly(vinylidene fluoride). *Macromolecules* **1980**, *13*, 1317–1318. [CrossRef]
42. Ramadan, K.S.; Sameoto, D.; Evoy, S. A review of piezoelectric polymers as functional materials for electromechanical transducers. *Smart Mater. Struct.* **2014**, *23*, 23. [CrossRef]
43. Lando, J.B.; Olf, H.G.; Peterlin, A. NMR and X-ray determination of the structure of poly(vinylidene fluoride). *J. Polym. Sci. Part A-1 Polym. Chem.* **1966**, *4*, 941–951. [CrossRef]
44. Rosenberg, Y.; Siegmann, A.; Narkis, M.; Shkolnik, S. The sol/gel contribution to the behavior of γ-irradiated poly(vinylidene fluoride). *J. Appl. Polym. Sci.* **1991**, *43*, 535–541. [CrossRef]
45. Lovinger, A.J. Annealing of poly(vinylidene fluoride) and formation of a fifth phase. *Macromolecules* **1982**, *15*, 40–44. [CrossRef]
46. Furukawa, T. Structure and Properties of Ferroelectric Polymers. *Key Eng. Mater.* **1994**, *92–93*, 15–30. [CrossRef]
47. Tashiro, K.; Takano, K.; Kobayashi, M.; Chatani, Y.; Tadokoro, H. Structural study on ferroelectric phase transition of vinylidene fluoride-trifluoroethylene copolymers (III) dependence of transitional behavior on VDF molar content. *Ferroelectrics* **1984**, *57*, 297–326. [CrossRef]
48. Tashiro, K.; Kobayashi, M. Structural phase transition in ferroelectric fluorine polymers: X-ray diffraction and infrared/Raman spectroscopic study. *Phase Transit.* **1989**, *18*, 213–246. [CrossRef]
49. Tashiro, K.; Takano, K.; Kobayashi, M.; Chatani, Y.; Tadokoro, H. Structural study on ferroelectric phase transition of vinylidene fluoride-trifluoroethylene random copolymers. *Polymer* **1981**, *22*, 1312–1314. [CrossRef]
50. Legrand, J.F.; Schuele, P.J.; Schmidt, V.H.; Minier, M. Nmr study of the ferroelectric phase transition in a 7030 mol% copolymer of vinylidene fluoride (VF2) and trifluoroethylene (TrFE). *Polymer* **1985**, *26*, 1683–1688. [CrossRef]
51. Bargain, F.; Panine, P.; Dos Santos, F.D.; Tencé-Girault, S. From solvent-cast to annealed and poled poly(VDF-co-TrFE) films: New insights on the defective ferroelectric phase. *Polymer* **2016**, *105*, 144–156. [CrossRef]
52. Capsal, J.-F.; Galineau, J.; Le, M.-Q.; Dos Santos, F.D.; Cottinet, P.-J. Enhanced electrostriction based on plasticized relaxor ferroelectric P(VDF-TrFE-CFE/CTFE) blends. *J. Polym. Sci. Part B Polym. Phys.* **2015**, *53*, 1368–1379. [CrossRef]
53. Qiao, B.; Wang, X.; Tan, S.; Zhu, W.; Zhang, Z. Synergistic Effects of Maxwell Stress and Electrostriction in Electromechanical Properties of Poly(vinylidene fluoride)-Based Ferroelectric Polymers. *Macromolecules* **2019**, *52*, 9000–9011. [CrossRef]
54. Bargain, F.; Thuau, D.; Hadziioannou, G.; Dos Santos, F.D.; Tencé-Girault, S. Phase diagram of poly(VDF-ter-TrFE-ter-CTFE) copolymers: Relationship between crystalline structure and material properties. *Polymer* **2021**, *213*, 123203. [CrossRef]
55. Bargain, F.; Thuau, D.; Panine, P.; Hadziioannou, G.; Dos Santos, F.D.; Tencé-Girault, S. Thermal behavior of poly(VDF-ter-TrFE-ter-CTFE) copolymers: Influence of CTFE termonomer on the crystal-crystal transitions. *Polymer* **2019**, *161*, 64–77. [CrossRef]
56. Gregorio, R. Determination of the α, β, and γ crystalline phases of poly(vinylidene fluoride) films prepared at different conditions. *J. Appl. Polym. Sci.* **2006**, *100*, 3272–3279. [CrossRef]
57. Lopes, A.C.; Costa, C.M.; Tavares, C.J.; Neves, I.C.; Lanceros-Mendez, S. Nucleation of the Electroactive γ Phase and Enhancement of the Optical Transparency in Low Filler Content Poly(vinylidene)/Clay Nanocomposites. *J. Phys. Chem. C* **2011**, *115*, 18076–18082. [CrossRef]
58. Davis, G.T.; McKinney, J.E.; Broadhurst, M.G.; Roth, S.C. Electric-field-induced phase changes in poly(vinylidene fluoride). *J. Appl. Phys.* **1978**, *49*, 4998–5002. [CrossRef]
59. Ghosh, S.K.; Alam, M.M.; Mandal, D. The in situ formation of platinum nanoparticles and their catalytic role in electroactive phase formation in poly(vinylidene fluoride): A simple preparation of multifunctional poly(vinylidene fluoride) films doped with platinum nanoparticles. *RSC Adv.* **2014**, *4*, 41886–41894. [CrossRef]
60. Bormashenko, Y.; Pogreb, R.; Stanevsky, O. Vibrational spectrum of PVDF and its interpretation. *Polym. Test.* **2004**, *23*, 791–796. [CrossRef]
61. Lanceros-Méndez, S.; Mano, J.F.; Costa, A.M.; Schmidt, V.H. Ftir and dsc studies of mechanically deformed β-pvdf films. *J. Macromol. Sci. Part B* **2001**, *40*, 517–527. [CrossRef]
62. Gregorio, J.R.; Cestari, M. Effect of crystallization temperature on the crystalline phase content and morphology of poly(vinylidene fluoride). *J. Polym. Sci. Part B Polym. Phys.* **1994**, *32*, 859–870. [CrossRef]
63. Salimi, A.; Yousefi, A. Analysis Method. *Polym. Test.* **2003**, *22*, 699–704. [CrossRef]
64. Li, J.C.; Wang, C.L.; Zhong, W.L.; Zhang, P.L.; Wang, Q.H.; Webb, J.F. Vibrational mode analysis of β-phase poly(vinylidene fluoride). *Appl. Phys. Lett.* **2002**, *81*, 2223–2225. [CrossRef]

65. Gregorio, R., Jr.; Capitão, R.C. Morphology and phase transition of high melt temperature crystallized poly(vinylidene fluoride). *J. Mater. Sci.* **2000**, *35*, 299–306. [CrossRef]
66. Cai, X.; Lei, T.; Sun, D.; Lin, L. A critical analysis of the α, β and γ phases in poly(vinylidene fluoride) using FTIR. *RSC Adv.* **2017**, *7*, 15382–15389. [CrossRef]
67. Sebastian, M.S.; Larrea, A.; Gonçalves, R.; Alejo, T.; Vilas, J.L.; Sebastian, V.; Martins, P.; Lanceros-Mendez, S. Understanding nucleation of the electroactive β-phase of poly(vinylidene fluoride) by nanostructures. *RSC Adv.* **2016**, *6*, 113007–113015. [CrossRef]
68. Tiwari, V.; Srivastava, G. Effect of thermal processing conditions on the structure and dielectric properties of PVDF films. *J. Polym. Res.* **2014**, *21*, 1–8. [CrossRef]
69. Wang, H.; Zhang, Q.M.; Cross, L.E.; Sykes, A.O. Piezoelectric, dielectric, and elastic properties of poly(vinylidene fluoride/trifluoroethylene). *J. Appl. Phys.* **1993**, *74*, 3394–3398. [CrossRef]
70. Aksel, E.; Jones, J.L. Advances in Lead-Free Piezoelectric Materials for Sensors and Actuators. *Sensors* **2010**, *10*, 1935–1954. [CrossRef]
71. Ribeiro, C.; Costa, C.M.; Correia, D.M.; Nunes-Pereira, J.; Oliveira, J.; Martins, P.; Gonçalves, R.; Cardoso, V.F.; Lanceros-Méndez, S. Electroactive poly(vinylidene fluoride)-based structures for advanced applications. *Nat. Protoc.* **2018**, *13*, 681–704. [CrossRef]
72. Farmer, B.L.; Hopfinger, A.J.; Lando, J.B. Polymorphism of poly(vinylidene fluoride): Potential energy calculations of the effects of head-to-head units on the chain conformation and packing of poly(vinylidene fluoride). *J. Appl. Phys.* **1972**, *43*, 4293–4303. [CrossRef]
73. Martins, P.; Nunes, J.S.; Hungerfordb, G.; Mirandaa, D.; Ferreira, A.; Sencadas, V.; Lanceros-Méndez, S. Local variation of the dielectric properties of poly(vinylidene fluoride) during the α- to β-phase transformation. *Phys. Lett. A* **2009**, *373*, 177–180. [CrossRef]
74. Chilibon, I.; Marat-Mendes, J.N. Ferroelectric ceramics by sol–gel methods and applications: A review. *J. Sol-Gel. Sci. Technol.* **2012**, *64*, 571–611. [CrossRef]
75. Ohigashi, H. Electromechanical properties of polarized polyvinylidene fluoride films as studied by the piezoelectric resonance method. *J. Appl. Phys.* **1976**, *47*, 949–955. [CrossRef]
76. Xu, H. Dielectric properties and ferroelectric behavior of poly(vinylidene fluoride-trifluoroethylene) 50/50 copolymer ultrathin films. *J. Appl. Polym. Sci.* **2001**, *80*, 2259–2266. [CrossRef]
77. Omote, K.; Ohigashi, H.; Koga, K. Temperature dependence of elastic, dielectric, and piezoelectric properties of "single crystalline" films of vinylidene fluoride trifluoroethylene copolymer. *J. Appl. Phys.* **1997**, *81*, 2760–2769. [CrossRef]
78. Koga, K.; Ohigashi, H. Piezoelectricity and related properties of vinylidene fluoride and trifluoroethylene copolymers. *J. Appl. Phys.* **1986**, *59*, 2142–2150. [CrossRef]
79. Cheng, Z.; Zhang, Q.; Su, J.; El Tahchi, M. Electropolymers for Mechatronics and Artificial Muscles. In *Piezoelectric and Acoustic Materials for Transducer Applications*; Springer: Berlin/Heidelberg, Germany, 2008; pp. 131–159.
80. Li, Z.; Wang, Y.; Cheng, Z.-Y. Electromechanical properties of poly(vinylidene-fluoride-chlorotrifluoroethylene) copolymer. *Appl. Phys. Lett.* **2006**, *88*, 062904. [CrossRef]
81. Crisler, D.; Cupal, J.; Moore, A. Dielectric, piezoelectric, and electromechanical coupling constants of zinc oxide crystals. *Proc. IEEE* **1968**, *56*, 225–226. [CrossRef]
82. Wang, H.; Chen, F.; Yu, F.; Lu, Q.; Li, Y.; Duan, X.; Zhang, S.; Zhao, X. Temperature dependence of the electro-elastic properties of the monoclinic α-BiB 3 O 6 crystals. *J. Alloy. Compd.* **2017**, *699*, 505–510. [CrossRef]
83. Chen, F.-F.; Yu, F.-P.; Bai, W.-Y.; Xiong, L.; Diebold, G.J.; Zhao, X. High Performance Piezoelectric Crystal Alpha-Bibo for Photoacoustic Gas Detection. In Proceedings of the 2019 13th Symposium on Piezoelectrcity, Acoustic Waves and Device Applications (SPAWDA), Harbin, China, 11–14 January 2019; pp. 1–4.
84. Huang, Y.; Rui, G.; Li, Q.; Allahyarov, E.; Li, R.; Fukuto, M.; Zhong, G.-J.; Xu, J.-Z.; Li, Z.-M.; Taylor, P.L.; et al. Enhanced piezoelectricity from highly polarizable oriented amorphous fractions in biaxially oriented poly(vinylidene fluoride) with pure β crystals. *Nat. Commun.* **2021**, *12*, 1–8. [CrossRef]
85. Fujisaki, S.; Ishiwara, H.; Fujisaki, Y. Low-voltage operation of ferroelectric poly(vinylidene fluoride-trifluoroethylene) copolymer capacitors and metal-ferroelectric-insulator-semiconductor diodes. *Appl. Phys. Lett.* **2007**, *90*, 162902. [CrossRef]
86. Li, Q.; Wang, Q. Ferroelectric Polymers and Their Energy-Related Applications. *Macromol. Chem. Phys.* **2016**, *217*, 1228–1244. [CrossRef]
87. Guo, H.; Wu, Q.; Sun, H.; Liu, X.; Sui, H. Organic phosphonic acid-modified BaTiO3/P(VDF-TrFE) composite with high output in both voltage and power for flexible piezoelectric nanogenerators. *Mater. Today Energy* **2020**, *17*, 100489. [CrossRef]
88. Ma, J.; Azhar, U.; Zong, C.; Zhang, Y.; Xu, A.; Zhai, C.; Zhang, L.; Zhang, S. Core-shell structured PVDF@BT nanoparticles for dielectric materials: A novel composite to prove the dependence of dielectric properties on ferroelectric shell. *Mater. Des.* **2019**, *164*, 107556. [CrossRef]
89. Martins, P.; Moya, X.; Phillips, L.C.; Kar-Narayan, S.; Mathur, N.D.; Lanceros-Mendez, S. Linear anhysteretic direct magnetoelectric effect in Ni0.5Zn0.5Fe2O4/poly(vinylidene fluoride-trifluoroethylene) 0-3 nanocomposites. *J. Phys. D Appl. Phys.* **2011**, *44*, 482001. [CrossRef]
90. Li, J.; Zhao, C.; Xia, K.; Liu, X.; Li, D.; Han, J. Enhanced piezoelectric output of the PVDF-TrFE/ZnO flexible piezoelectric nanogenerator by surface modification. *Appl. Surf. Sci.* **2019**, *463*, 626–634. [CrossRef]

91. Yang, T.; Pan, H.; Tian, G.; Zhang, B.; Xiong, D.; Gao, Y.; Yan, C.; Chu, X.; Chen, N.; Zhong, S.; et al. Hierarchically structured PVDF/ZnO core-shell nanofibers for self-powered physiological monitoring electronics. *Nano Energy* **2020**, *72*, 104706. [CrossRef]
92. Arshad, A.N.; Wahid, M.H.M.; Rusop, M.; Majid, W.H.A.; Subban, R.H.Y.; Rozana, M.D. Dielectric and Structural Properties of Poly(vinylidene fluoride) (PVDF) and Poly(vinylidene fluoride-trifluoroethylene) (PVDF-TrFE) Filled with Magnesium Oxide Nanofillers. *J. Nanomater.* **2019**, *2019*, 1–12. [CrossRef]
93. Mandal, D.; Kim, K.J.; Lee, J.S. Simple Synthesis of Palladium Nanoparticles, β-Phase Formation, and the Control of Chain and Dipole Orientations in Palladium-Doped Poly(vinylidene fluoride) Thin Films. *Langmuir* **2012**, *28*, 10310–10317. [CrossRef]
94. Roy, K.; Ghosh, S.K.; Sultana, A.; Garain, S.; Xie, M.; Bowen, C.R.; Henkel, K.; Schmeißer, D.; Mandal, D. A Self-Powered Wearable Pressure Sensor and Pyroelectric Breathing Sensor Based on GO Interfaced PVDF Nanofibers. *ACS Appl. Nano Mater.* **2019**, *2*, 2013–2025. [CrossRef]
95. Bhavanasi, V.; Kumar, V.; Parida, K.; Wang, J.; Lee, P.S. Enhanced Piezoelectric Energy Harvesting Performance of Flexible PVDF-TrFE Bilayer Films with Graphene Oxide. *ACS Appl. Mater. Interfaces* **2016**, *8*, 521–529. [CrossRef] [PubMed]
96. Patro, T.U.; Mhalgi, M.V.; Khakhar, D.V.; Misra, A. Studies on poly(vinylidene fluoride)–clay nanocomposites: Effect of different clay modifiers. *Polymer* **2008**, *49*, 3486–3499. [CrossRef]
97. Li, T.; Qu, M.; Carlos, C.; Gu, L.; Jin, F.; Yuan, T.; Wu, X.; Xiao, J.; Wang, T.; Dong, W.; et al. High-Performance Poly(vinylidene difluoride)/Dopamine Core/Shell Piezoelectric Nanofiber and Its Application for Biomedical Sensors. *Adv. Mater.* **2020**, *33*, e2006093. [CrossRef] [PubMed]
98. Liu, Y.; Yang, T.; Zhang, B.; Williams, T.; Lin, Y.; Li, L.; Zhou, Y.; Lu, W.; Kim, S.H.; Chen, L.; et al. Structural Insight in the Interfacial Effect in Ferroelectric Polymer Nanocomposites. *Adv. Mater.* **2020**, *32*, e2005431. [CrossRef]
99. Chen, Q.; Shen, Y.; Zhang, S.; Zhang, Q. Polymer-Based Dielectrics with High Energy Storage Density. *Annu. Rev. Mater. Res.* **2015**, *45*, 433–458. [CrossRef]
100. Dudem, B.; Kim, D.H.; Bharat, L.K.; Yu, J.S. Highly-flexible piezoelectric nanogenerators with silver nanowires and barium titanate embedded composite films for mechanical energy harvesting. *Appl. Energy* **2018**, *230*, 865–874. [CrossRef]
101. Ma, W.; Zhang, J.; Wang, X. Effect of Initial Polymer Concentration on the Crystallization of Poly (Vinylidene Fluoride)/Poly (Methyl Methacrylate) Blend from Solution Casting. *J. Macromol. Sci. Part B* **2007**, *47*, 139–149. [CrossRef]
102. Zhang, C.; Fan, Y.; Li, H.; Li, Y.; Zhang, L.; Cao, S.; Kuang, S.; Zhao, Y.; Chen, A.; Zhu, G.; et al. Fully Rollable Lead-Free Poly(vinylidene fluoride)-Niobate-Based Nanogenerator with Ultra-Flexible Nano-Network Electrodes. *ACS Nano* **2018**, *12*, 4803–4811. [CrossRef]
103. Cardoso, V.F.; Costa, C.M.; Minas, G.; Lanceros-Mendez, S. Improving the optical and electroactive response of poly(vinylidene fluoride–trifluoroethylene) spin-coated films for sensor and actuator applications. *Smart Mater. Struct.* **2012**, *21*, 21. [CrossRef]
104. Choi, M.; Murillo, G.; Hwang, S.; Kim, J.W.; Jung, J.H.; Chen, C.-Y.; Lee, M. Mechanical and electrical characterization of PVDF-ZnO hybrid structure for application to nanogenerator. *Nano Energy* **2017**, *33*, 462–468. [CrossRef]
105. Yaqoob, U.; Habibur, R.M.; Sheeraz, M.; Kim, H.C. Realization of self-poled, high performance, flexible piezoelectric energy harvester by employing PDMS-rGO as sandwich layer between P(VDF-TrFE)-PMN-PT composite sheets. *Compos. Part B Eng.* **2019**, *159*, 259–268. [CrossRef]
106. Zhang, L.; Liu, H.; Zhao, Y.; Sun, X.; Wen, Y.; Guo, Y.; Gao, X.; Di, C.-A.; Yu, G.; Liu, Y. Inkjet Printing High-Resolution, Large-Area Graphene Patterns by Coffee-Ring Lithography. *Adv. Mater.* **2011**, *24*, 436–440. [CrossRef]
107. Pabst, O.; Perelaer, J.; Beckert, E.; Schubert, U.S.; Eberhardt, R.; Tünnermann, A. All inkjet-printed piezoelectric polymer actuators: Characterization and applications for micropumps in lab-on-a-chip systems. *Org. Electron.* **2013**, *14*, 3423–3429. [CrossRef]
108. Thuau, D.; Kallitsis, K.; Dos Santos, F.D.; Hadziioannou, G. All inkjet-printed piezoelectric electronic devices: Energy generators, sensors and actuators. *J. Mater. Chem. C* **2017**, *5*, 9963–9966. [CrossRef]
109. Zirkl, M.; Sawatdee, A.; Helbig, U.; Krause, M.; Scheipl, G.; Kraker, E.; Ersman, P.A.; Nilsson, D.; Platt, D.; Bodö, P.; et al. An All-Printed Ferroelectric Active Matrix Sensor Network Based on Only Five Functional Materials Forming a Touchless Control Interface. *Adv. Mater.* **2011**, *23*, 2069–2074. [CrossRef]
110. Correia, D.M.; Ribeiro, C.; Sencadas, V.; Vikingsson, L.; Gasch, M.O.; Ribelles, J.L.G.; Botelho, G.; Lanceros-Méndez, S. Strategies for the development of three dimensional scaffolds from piezoelectric poly(vinylidene fluoride). *Mater. Des.* **2016**, *92*, 674–681. [CrossRef]
111. Kallitsis, K.; Thuau, D.; Soulestin, T.; Brochon, C.; Cloutet, E.; Dos Santos, F.D.; Hadziioannou, G. Photopatternable High-k Fluoropolymer Dielectrics Bearing Pendent Azido Groups. *Macromolecules* **2019**, *52*, 5769–5776. [CrossRef]
112. Shirinov, A.V.; Schomburg, W.K. Pressure sensor from a PVDF film. *Sens. Actuators A Phys.* **2008**, *142*, 48–55. [CrossRef]
113. Toda, M.; Thompson, M. Contact-Type Vibration Sensors Using Curved Clamped PVDF Film. *IEEE Sens. J.* **2006**, *6*, 1170–1177. [CrossRef]
114. Li, Q.; Ke, W.; Chang, T.; Hu, Z. A molecular ferroelectrics induced electroactive β-phase in solution processed PVDF films for flexible piezoelectric sensors. *J. Mater. Chem. C* **2019**, *7*, 1532–1543. [CrossRef]
115. Xiong, Y.; Shen, Y.; Tian, L.; Hu, Y.; Zhu, P.; Sun, R.; Wong, C.-P. A flexible, ultra-highly sensitive and stable capacitive pressure sensor with convex microarrays for motion and health monitoring. *Nano Energy* **2020**, *70*, 104436. [CrossRef]
116. Guo, Z.; Liu, S.; Hu, X.; Zhang, Q.; Shang, F.; Song, S.; Xiang, Y. Self-powered sound detection and recognition sensors based on flexible polyvinylidene fluoride-trifluoroethylene films enhanced by in-situ polarization. *Sens. Actuators A Phys.* **2020**, *306*, 111970. [CrossRef]

117. Evans, A.M.; Bradshaw, N.P.; Litchfield, B.; Strauss, M.J.; Seckman, B.; Ryder, M.R.; Castano, I.; Gilmore, C.; Gianneschi, N.C.; Mulzer, C.R.; et al. High-Sensitivity Acoustic Molecular Sensors Based on Large-Area, Spray-Coated 2D Covalent Organic Frameworks. *Adv. Mater.* **2020**, *32*. [CrossRef]
118. Lang, C.; Fang, J.; Shao, H.; Ding, X.; Lin, T. High-sensitivity acoustic sensors from nanofibre webs. *Nat. Commun.* **2016**, *7*, 11108. [CrossRef]
119. Han, J.H.; Kwak, J.-H.; Joe, D.J.; Hong, S.K.; Wang, H.S.; Park, J.H.; Hur, S.; Lee, K.J. Basilar membrane-inspired self-powered acoustic sensor enabled by highly sensitive multi tunable frequency band. *Nano Energy* **2018**, *53*, 198–205. [CrossRef]
120. Hu, J.; Peng, H.; Yao, X. Design of PVDF sensor array for determining airflow direction and velocity. *Rev. Sci. Instrum.* **2018**, *89*, 085007. [CrossRef] [PubMed]
121. Son, H.Y.; Park, J.S.; Huang, J.; Kim, J.; Nam, Y.S.; Kim, W.S. Flexible Fibrous Piezoelectric Sensors on Printed Silver Electrodes. *IEEE Trans. Nanotechnol.* **2014**, *13*, 709–713. [CrossRef]
122. Chang, J.; Lin, L. Large array electrospun PVDF nanogenerators on a flexible substrate. In Proceedings of the 2011 16th International Solid-State Sensors, Actuators and Microsystems Conference, Beijing, China, 5–9 June 2011; pp. 747–750.
123. Wang, W.; Stipp, P.N.; Ouaras, K.; Fathi, S.; Huang, Y.Y.S. Broad Bandwidth, Self-Powered Acoustic Sensor Created by Dynamic Near-Field Electrospinning of Suspended, Transparent Piezoelectric Nanofiber Mesh. *Small* **2020**, *16*, e2000581. [CrossRef]
124. Tuloup, C.; Harizi, W.; Aboura, Z.; Meyer, Y.; Khellil, K.; Lachat, R. On the use of in-situ piezoelectric sensors for the manufacturing and structural health monitoring of polymer-matrix composites: A literature review. *Compos. Struct.* **2019**, *215*, 127–149. [CrossRef]
125. Chilles, J.S.; Koutsomitopoulou, A.F.; Croxford, A.J.; Bond, I.P. Monitoring cure and detecting damage in composites with inductively coupled embedded sensors. *Compos. Sci. Technol.* **2016**, *134*, 81–88. [CrossRef]
126. Caneva, C.; De Rosa, I.; Sarasini, F. Monitoring of Impacted Aramid-Reinforced Composites by Embedded PVDF Acoustic Emission Sensors. *Strain* **2008**, *44*, 308–316. [CrossRef]
127. De Rosa, I.; Sarasini, F. Use of PVDF as acoustic emission sensor for in situ monitoring of mechanical behaviour of glass/epoxy laminates. *Polym. Test.* **2010**, *29*, 749–758. [CrossRef]
128. Park, J.-M.; Kong, J.-W.; Kim, D.-S.; Yoon, D.-J. Nondestructive damage detection and interfacial evaluation of single-fibers/epoxy composites using PZT, PVDF and P(VDF-TrFE) copolymer sensors. *Compos. Sci. Technol.* **2005**, *65*, 241–256. [CrossRef]
129. Wang, Z.L. Piezoelectric Nanogenerators Based on Zinc Oxide Nanowire Arrays. *Science* **2006**, *312*, 242–246. [CrossRef]
130. Mutsuda, H.; Tanaka, Y.; Patel, R.; Doi, Y. Harvesting flow-induced vibration using a highly flexible piezoelectric energy device. *Appl. Ocean Res.* **2017**, *68*, 39–52. [CrossRef]
131. Shan, X.; Tian, H.; Chen, D.; Xie, T. A curved panel energy harvester for aeroelastic vibration. *Appl. Energy* **2019**, *249*, 58–66. [CrossRef]
132. Mokhtari, F.; Foroughi, J.; Zheng, T.; Cheng, Z.; Spinks, G.M. Triaxial braided piezo fiber energy harvesters for self-powered wearable technologies. *J. Mater. Chem. A* **2019**, *7*, 8245–8257. [CrossRef]
133. Lee, M.; Chen, C.-Y.; Wang, S.; Cha, S.N.; Park, Y.J.; Kim, J.M.; Chou, L.-J.; Wang, Z.L. A Hybrid Piezoelectric Structure for Wearable Nanogenerators. *Adv. Mater.* **2012**, *24*, 1759–1764. [CrossRef]
134. Huang, T.; Wang, C.; Yu, H.; Wang, H.; Zhang, Q.; Zhu, M. Human walking-driven wearable all-fiber triboelectric nanogenerator containing electrospun polyvinylidene fluoride piezoelectric nanofibers. *Nano Energy* **2015**, *14*, 226–235. [CrossRef]
135. Liu, J.; Yang, B.; Lu, L.; Wang, X.; Li, X.; Chen, X.; Liu, J. Flexible and lead-free piezoelectric nanogenerator as self-powered sensor based on electrospinning BZT-BCT/P(VDF-TrFE) nanofibers. *Sens. Actuators A Phys.* **2020**, *303*, 111796. [CrossRef]
136. Jella, V.; Ippili, S.; Eom, J.-H.; Choi, J.; Yoon, S.-G. Enhanced output performance of a flexible piezoelectric energy harvester based on stable MAPbI3-PVDF composite films. *Nano Energy* **2018**, *53*, 46–56. [CrossRef]
137. Hoque, N.A.; Thakur, P.; Biswas, P.; Saikh, M.; Roy, S.; Bagchi, B.; Das, S.; Ray, P.P. Biowaste crab shell-extracted chitin nanofiber-based superior piezoelectric nanogenerator. *J. Mater. Chem. A* **2018**, *6*, 13848–13858. [CrossRef]
138. Ribeiro, C.; Moreira, S.; Correia, V.; Sencadas, V.; Rocha, J.; Gama, F.M.; Ribelles, J.L.G.; Lanceros-Méndez, S. Enhanced proliferation of pre-osteoblastic cells by dynamic piezoelectric stimulation. *RSC Adv.* **2012**, *2*, 11504–11509. [CrossRef]
139. Rodrigues, M.T.; Gomes, M.; Mano, J.F.; Reis, R.L. β-PVDF Membranes Induce Cellular Proliferation and Differentiation in Static and Dynamic Conditions. *Mater. Sci. Forum* **2008**, *587–588*, 72–76. [CrossRef]
140. Zhang, X.; Zhang, C.; Lin, Y.; Hu, P.; Shen, Y.; Wang, K.; Meng, S.; Chai, Y.; Dai, X.; Liu, X.; et al. Nanocomposite Membranes Enhance Bone Regeneration Through Restoring Physiological Electric Microenvironment. *ACS Nano* **2016**, *10*, 7279–7286. [CrossRef]